

Effect of observer perspective on the perception of wavelength

Richard K. Love ^{*a} and Sean R. Love ^{†b}

^a 2000 Clara Mae Ct. Springfield IL 62711

^b 191 East El Camino Real, Mountain View CA 94040

(Dated Jun 3, 2013)

PACS numbers: 03.30.+p 95.30.Sf, 98.80.Jk 5.35+d, 95.38.+x, 95.55.Pe, 98.80.bp, 98.80.es, 98.80.-k, 98.80HW

Electronic address: richlove@scientificdatallc.com

Electronic address: seanlove@scientificdatallc.com

Abstract

The redshift observed in astronomical measurements is explained as an observational artifact caused by the perspective of the observer, rather than the effect of physical cosmic expansion. The parsec unit of distance is defined in the observer-centered perspective, which is the generic term for the geocentric perspective. This perspective uses taxicab geometry which causes the Earth observer to perceive a longer wavefront travel distance for the parsec unit without a corresponding increase in wavefront travel time. This combination creates a velocity artifact v_a , which, since it is part of each parsec unit, is cumulative with distance. The velocity artifact manifests to the Earth observer as an apparent redshift which only becomes significant at the megaparsec level. Predicted results are very close to expected values. The predicted Hubble constant value is calculated to be 69.4, 70, and 69.3 $km/s/Mpc$ depending on which formula is used. Each of the three values is within NASA's limits. The artifact is also shown to generate the sinusoidal FRW wave functions for recession velocity, redshift and the scale factor. The artifact predicts a recession velocity of $1c$ to equal a redshift of 1.46, which equals the expected redshift value. The artifact is also demonstrated to be responsible for the phenomena commonly known as dark energy by causing objects to appear closer than expected due to shorter redshift-distance.. Riess et al (2004) found the redshift distance to be shorter by 10 to 15%. Correction of the artifact error causes the FRW redshift luminosity distance to increase by 14% which can be seen to closely match the intrinsic luminosity distance of the type 1a supernovae (SNe Ia). . The Pioneer anomaly, which is the unmodeled negative acceleration of two spacecraft launched in 1972, is also shown to be the result of the observer-centered perspective. The calculated negative acceleration of $-8.745 \times 10^{-10} km/s/s$ essentially equals NASA's value

I. ALIGNMENT OF THE EARTH AND SUN WITH A STAR OR GALAXY

A. Effects of perspective on properties of wavefront

In 1534, Copernicus discovered a new perspective for observation within the solar system, which is known today as the heliocentric perspective [1]. This perspective is

generically termed the *source-centered perspective* when applied to other light sources.

[2] The source-centered perspective measures distance from the origin of the wavefront of light, such as a star or galaxy. It uses the polar coordinate system, with the radial coordinate r and the transverse coordinate θ and is individually aligned with the light source.

When r is expressed in the 2-norm metric of this perspective, coordinates y and x combine to form the defined radial line ($r = \sqrt{y^2 + x^2}$). The distance r also is the total distance from the star to Earth. [3] The relationship between incremental radial and transverse distance is given by the formula $\Delta r = \Delta C / 2\pi$: where Δr is the incremental radial distance and ΔC is an incremental change in the Euclidean wavefront circumference. [4]

Prior to Copernicus, observers measured planetary distances in the solar system from the origin on the Earth with a perspective known today as the as geocentric perspective. [5]. This perspective is generically termed the *observer-centered perspective* when applied to other light sources. It measures distance from the origin of the observer. [6]

The perspective uses the Cartesian coordinate system, which aligns the radial coordinate y and the transverse coordinate x with the origin of the observer. The particular alignment of the coordinate axes with the wavefront that is perceived by the observer is applied to all other objects. [7]

As expressed in the 1-norm metric of this perspective, coordinates y and x cannot combine to form a radial line because y is the defined radial distance and x is the defined transverse distance. In this metric, they can only *add* to give the total distance ($x + y$) from the Earth to the star. [8] The relationship between incremental radial and transverse distance is given by the formula $\Delta y = \Delta x / \tan \theta$: where Δy is the incremental radial distance and Δx is the incremental change in the taxicab wavefront circumference. [9] [10] [11]

Table 1 summarizes the properties of each perspective.

Perspective Name	Coordinate origin	Coordinate system	Minkowski geometry	Incremental radial distance
Source-centered	Star or galaxy	Polar	Euclidean*	$\Delta r = \Delta C / 2\theta$
Observer-centered	Observer	Cartesian	Taxicab	$\Delta y = \Delta x / \tan \theta$

Table 1: A summary of the properties of the source-centered and observer-centered perspectives *As discussed, the polar distance r can be expressed as Euclidean distance ($\sqrt{y^2 + x^2}$) [12]

B. Example of the source-centered perspective

In the example in FIG.1, the Sun S and the Earth E are aligned so that the wavefront distance ct from the star is equal for both objects. As mentioned, the source-centered perspective uses polar coordinates. The radial and transverse directions are defined spectroscopically, that is by their effect on wavelength as measured by a moving observer. [13]

Spectroscopically, the outward direction from the star along the ray of light is defined as radial because travel in this direction causes a change in wave travel distance ct which results in a change in wavelength.

The orthogonal direction to the radial coordinate (r) is the arc s which is the product of the two coordinates $r\theta$. The arc, seen between the Sun S and an Earth orbit position E is defined spectroscopically as transverse because travel in this direction does not result in a change in wave travel distance ct so there is no observed change in wavelength.

As can be seen, each ray from the Sun S is individually aligned with the transverse distance. Since only the curved wavefront can be truly transverse to the radial direction, it follows that a rectilinear “transverse” distance necessarily contains a radial component and thus would not meet the spectroscopic test of being transverse.

The accepted distance between the Earth and the Sun is the radar-measured chord l , which, with a small angle θ , closely approximates the arc. Since the angle used in this paper is very small (one arcsecond), the radar magnitude of the chord will be used in calculations as the magnitude of the arc. The chord, like the arc, generates no net radial displacement between the Sun and the Earth. [14]

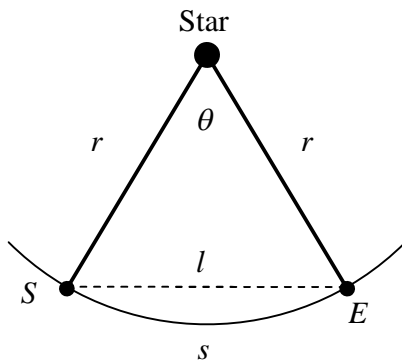


FIG.1: The source-centered perspective, uses the polar coordinates r and θ , and has its origin on the source (star). Equidistance is measured in wavefront travel distance r . The Sun S and the Earth E each has its own individual alignment with the wavefront.

C. Example of intermediate step from source-centered to observer-centered perspective.

FIG.2 illustrates the intermediate step between the two perspectives. This step maintains the coordinate origin on the star and the individual alignment of the radial distance of the source centered perspective, but replaces the polar coordinate system with the Cartesian coordinate system.

Since the x distance is rectilinear, it is only truly in the spectroscopic transverse direction at the tangent point. The arc s can be thought to be composed of a series of infinitesimal rectilinear distances dl that are each tangential to an individual light ray. [16] [17]

The geometry remains Euclidean; as can be seen the radial distance from the star is point-to-point for both the Sun S and the Earth E . In this special case where the limit of the transverse distance x equals 0, then the radial distance y is calculated $\sqrt{y^2 + 0^2}$.

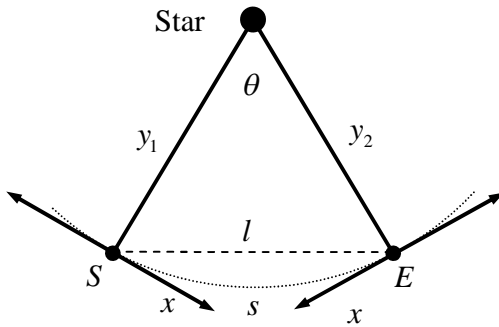


FIG.2: The intermediate stage between the source-centered and observer-centered perspective maintains both the origin on the star and the individual alignment with the wavefront. However, it uses Cartesian coordinates. Note that y_1 and y_2 are both equal to the wavefront travel distance r seen in FIG.1. Also note that the x coordinate is tangential and not completely transverse as is the curved arc s . Therefore x , because it is rectilinear, has a radial component.

D. Observer-centered perspective example

As was seen in FIG. 2, the alignment with the wavefront in the source-centered perspective was individually determined by each object. Now as seen in FIG. 3(a), the

alignment for all objects is instead determined by the *observer*. This difference in alignment with the wavefront changes the geometry in this perspective from Euclidean geometry to taxicab geometry, which in turn alters the direction and magnitude of the radial and transverse distances between the Sun, Earth and star.

In FIG.3 (a), the origin of distance is on the Sun S which is the observer. Note that the radial distance (y_2) from the Earth to the star no longer is equal to r which is a 2-norm distance ((difference between both x and y coordinates). Instead the radial distance y_2 is now equal to $r \cos \theta$, which is a 1-norm distance (difference between only one coordinate). In this case, the one coordinate is y . [18]

As can be seen, the Euclidean distances l and r are *undefined* in terms of radial and transverse distance. This is because it is the distance y that is *defined* as radial and the distance x that is *defined* as transverse. In this perspective, l and r are a combination of radial and transverse distances.

In this view, the Sun and the Earth each have different radial distances from the star as measured by y as the taxicab radial distance. For the Earth to have the same taxicab radial distance to the star as the Sun, it needs a different orbit position so that the y coordinate values of the Sun and the Earth are the same. This alignment is seen in FIG. 3(b).

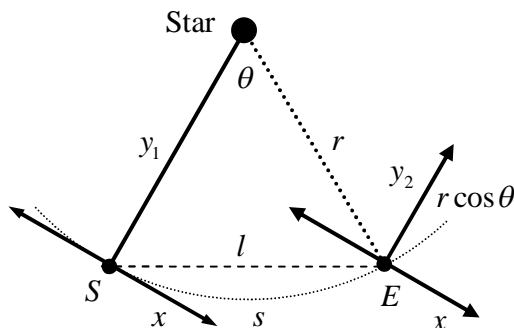


FIG.3 (a): The observer-centered perspective creates a common alignment with the wavefront for all objects based on the observer's view (which is the Sun S in this example). The magnitude of Earth E 's radial distance (y_2) to the star is no longer equal to the Euclidean distance (r), as it was in FIG. 2, instead it is now equal to the taxicab distance ($r \cos \theta$).

In FIG. 3 (b), the overlay of the wavefront from the Sun S makes it possible to see both the polar and Cartesian coordinate systems at the same time.

In taxicab geometry, the y coordinate is the sole component of radial direction. Thus, to have the Earth and the Sun at the same distance to the star requires the alignment of the Sun and Earth such that they both have the same y distance to the star. This alignment had the opposite effect in the Euclidean geometry; instead of being equal distance, the Earth is now at a greater r distance than the Sun. [19]

In the source-centered perspective, where radial distance is measured in terms of r , the x distance now has a change in wavefront travel distance from the star Δct , because, as can be seen, the Sun and the Earth have different radii.

However, in the observer-centered perspective, where radial distance is measured in terms of y , the x line has no change in radial distance; the Sun and the Earth have the same y distance. In this perspective, it is the l distance that has the change in radial distance Δct , because its beginning and end have different y values. [20]

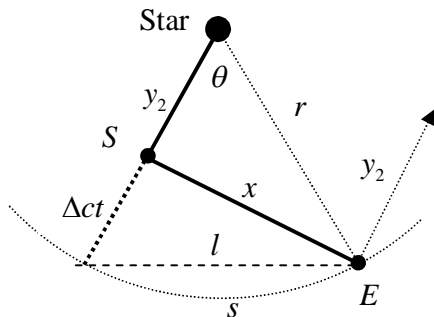


FIG.3 (b): The Earth E and the Sun S now have the same 1-norm radial distance (y_2) to the star. The realignment has caused x to add a radial component Δct in the source-centered perspective. However, in the observer-centered perspective, it is l that appears to have the radial component.

FIG. 3(c) is rotated to the familiar observer-centered position where y is vertical. Using the spectroscopic test, movement along s or l generates *no* net change in wavelength while movement along x does cause a net change.. Therefore x is not all transverse, it has a radial component. [21]

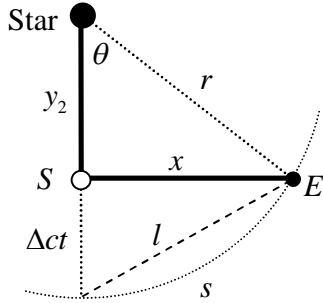


FIG.3 (c): The view is rotated to the normal Cartesian position. The arc s (approximated by the sum of the infinitesimal dl) is the spectroscopic transverse distance. Therefore it is x that has the radial component Δct . However, the Pythagorean equation $x^2 = dl^2 - (cdt)^2$ assumes that it is dl that has the radial component since l has

The Pythagorean equation $dx^2 = dl^2 - (cdt)^2$ is invalid for use with a point source of light because it doesn't follow the spectroscopic definitions of radial and transverse directions. The Pythagorean equation assumes that it is l that has the radial component. It can be seen in FIG. 3(c), that this assumption is made because l begins and ends with a different y coordinate value. [22] However, as has shown in FIG. 3(b), it is x that actually has the radial component, as measured spectroscopically.

II. REDSHIFT ARTIFACT IS CAUSED BY DIFFERENCE IN PERSPECTIVES.

A. Definition of the parsec in taxicab geometry

In FIG. 4, the Earth E is aligned to have the same taxicab radial distance y as the Sun S , which is required by the parallax equation because it uses the $1-norm$ metric.

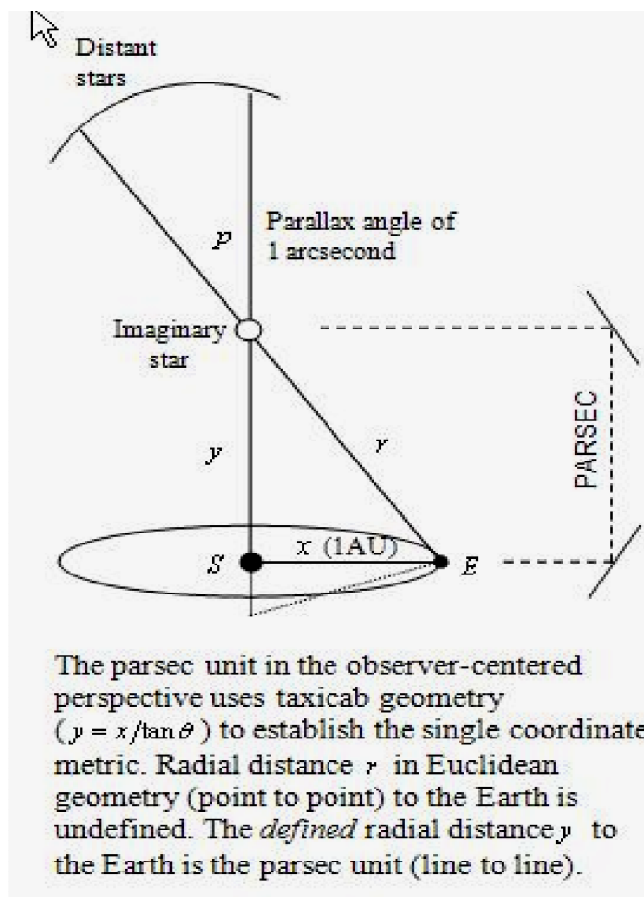
The definition of the parsec (pc) as the unit of radial distance is an excellent demonstration of the difference between Euclidean and taxicab geometry. As can be seen in FIG.4, the Euclidean radial distance r (point to point) from the star to the Earth is undefined, because the *defined* radial distance from the star to the Earth is the parsec y (line to line).

In the observer-centered perspective, the relationship between incremental change in between transverse and radial distance is defined by the parallax formula [23] [24]

$$pc(y) = \frac{x}{\tan p} \quad (1)$$

where y is the parsec, the magnitude of the baseline x is one AU and the magnitude of angle p is one arc second. (Note the very small angle (one arc second) that is actually used in the parsec determination; the larger angles in the diagrams are for ease of viewing).

Note in FIG.4, that the defined wavefront travel time from the imaginary star to the Earth is the parsec (y) divided by the speed of light ($t = y/c$). In comparison, the actual wavefront travel time from the imaginary star to the Earth is the radius r divided by the speed of light. ($t = r/c$).



In taxicab geometry, y/c may be called the “coordinate” time because all points on the x axis have the same y coordinate wavefront travel distance to the star by definition. In Euclidean geometry, r/c may be called the “proper” time, because each position on the

x axis has a unique r wavefront travel distance to the star. The term proper is used in this case with the definition “belonging to one: own. [25]

Note that the physical speed of light in a vacuum is accepted unconditionally in this paper as a constant in the universe. However, the magnitude of the variable c obviously depends on the magnitude of the distance unit used in its definition. [26]

The artifact velocity v_a is the difference between c calculated with the parsec distance y and c calculated using the actual distance to the Earth r . The proper time r/c was used for both calculations because it is the time used by the Earth observer.

$$v_a = \frac{r}{r/c} - \frac{y}{r/c} \quad (2)$$

Dividing through by the denominators, simplifies the equation

$$v_a = c - cy/r \quad (3)$$

Then the speed of light c can be factored to further simplify the equation.

$$v_a = c(1 - y/r) . \quad (4)$$

As can be seen in FIG. 4, the distance y is the adjacent side of the triangle and r is the hypotenuse of the triangle, therefore, the ratio y/r can be expressed as the cosine function, when angle $p = \theta$

$$v_a = c(1 - \cos \theta) . \quad (5)$$

As will be seen later in FIG.14, this function meets the expected curve shape for Doppler redshift when the recession velocity is divided by the speed of light (v_a/c).

The artifact velocity v_a is observed by the Earth observer as an apparent increase in the wavelength with the Doppler formula

$$\lambda_{obs} = (c + v_a)T . \quad (6)$$

The wavelength with this artifact velocity is referred to as the observed wavelength. The same wavelength without the artifact velocity is referred to as the emitted wavelength.

Note that simple movement by the star or the Earth would not explain the fact that the redshift is observed in all directions. However the velocity artifact, like the current

It can be seen in FIG.5 that the Sun and the Earth perceive different wavefront distances y and r and therefore perceive different wavelengths. However, it is easier to see that the Sun S and the Earth E have different wavelengths in FIG.6 where both wavefronts are Euclidean.

If the frequency ν of light from the star is set to 1, then for the Sun, the radius r_S equals λ_e but for the Earth, radius r_E equals λ_o . The two radii equal different wavelengths because they have the same wavefront travel time as set by the parsec.

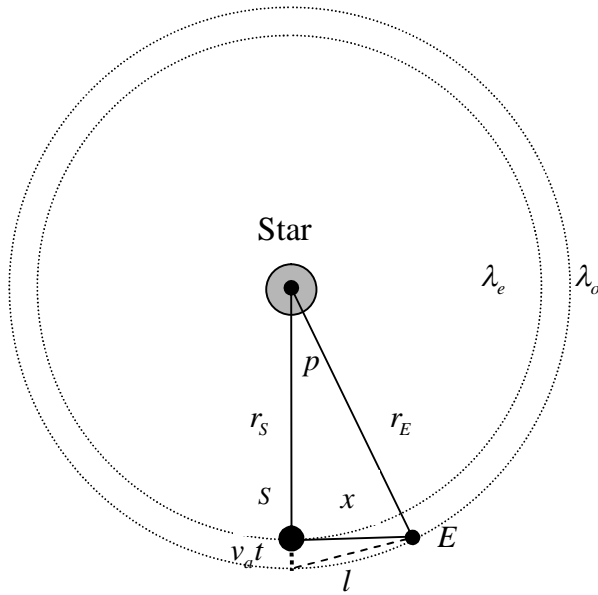


FIG.6 shows the two Euclidean wavefronts with radius r . In this geometry, the x distance has a radial component, so that the Sun S and the Earth E each have a different radius. Since the distance unit is defined in the taxicab metric, the wavefront travel time for both radii is the same, causing the Earth observer to perceive the artifact wavelength λ_o , caused by the artifact velocity v_a .

The increase in circumference between the two wavefront circles can be calculated by the difference in magnitude between the Euclidean chord l and the taxicab chord x . ($\Delta C = (l - x)$) The increase in circumference can then be related to an increase in radius by the equation,

$$\Delta r = \frac{\Delta C}{2\pi} \tag{7}$$

The change in the radius when traversed by light in the same time is explained as an increase in velocity ($c + v_a$). The artifact velocity v_a then causes the artifact wavelength λ_o .

C. Effect of an incremental increase in circumference on the radius

Astronomers have long believed that the small difference in transverse distance between x and l was insignificant because of the relatively large magnitude of the parsec. The effect is called the “skinny isosceles triangle”. [33] However, as the following example will demonstrate, an incremental change is not affected by the magnitude of the distance being changed.

A string that fits tightly around the Earth's circumference at the equator has a length of approximately 132 million feet (25,000 miles x 5,280 ft). If only sixty feet is added to the string's 132 million feet length, it provides enough slack to lift the string to a height of *ten feet* off the ground all around the world. [34]

Type	Function	Formula	Values (ft)
Increased circumference	C_{incr}	$C_{orig} + 60$	132,000,060
Original circumference	C_{orig}	C_{orig}	132,000,000
	ΔC	$(C_{incr} - C_{orig})$	60
	Δr	$\Delta C / 2\pi$	10

Table 2. An incremental increase in circumference of 60 ft. causes an incremental increase in radius of 10ft. ($2\pi \approx 6$)

This relationship of the circumference to the radius is surprising because the radius increase was expressed numerically as 60 feet rather than in terms of the percentage of the radius (4.76×10^{-7}) as was expected. Incrementally, every unit increase in circumference causes an $0.16 (1/2\pi)$ increase in radius.

An incremental increase is not affected by the magnitude of the distance hence, percentages are not appropriate in the calculation. This incremental effect combined with the fact that the parsec is a distance unit, means that the small differences in calculating transverse distance can be significant. This will be now demonstrated using the difference between the Euclidean circumference and the taxicab circumference as seen in FIG. 6.

The same equation used with the string can be used to determine the increase in radial distance caused by the difference in ΔC between the two perspectives. As previously discussed, the magnitude of the chord will be used for ΔC .

The difference in the circumference ΔC between the two perspectives is determined by subtraction of the taxicab chord x from the Euclidean chord l .

$$\Delta C = 2ct \sin \frac{\theta}{2} - AU \quad (8)$$

This increase in circumference can be used to determine the artifact velocity v_a with the following equation

$$v_a = \frac{\Delta C}{2\pi} \quad (9)$$

Where the arcsecond $\theta = 4.8481368111 \times 10^{-6}$ radians, $AU = 149,597,870.7 \text{ km}$ and $ct = 3.08567758100 \times 10^{13} \text{ km}$

Perspective	Function	Formula	Values (km / s)
Source-centered	d	$2ct \sin(\theta/2)$	149,597,870.700440
Observer-centered	x	AU	149,597,870.700000
	ΔC	$2ct \sin(\theta/2) - AU$	0.00440
	v_a	$\Delta C/2\pi$	0.000070

Table 3. The apparent increase in circumference for one parsec is 0.000440 km. Dividing 440 km by 2π gives the apparent recession velocity v_a of $7.0 \times 10^{-5} \text{ km/s/pc}$.

The magnitude of v_a per megaparsec is obtained by multiplying the magnitude of the artifact velocity value for the parsec by a factor of one million. The recession velocity artifact v_a at a one megaparsec level is known as the Hubble constant H_0

$$H_0 = 70 \text{ km/s/Mpc} \quad (10)$$

Edwin Hubble reported in 1927 that galaxies showed a redshift in their wavelengths that was proportional to their distance away from Earth. The quantitative correlation he developed based on this relationship is known as Hubble's law. [35]

Hubble's law describes the recession velocity v_r as a function of the distance between the observer and the object.

$$v_r = H_0 D \quad (11)$$

D , measured in mega parsecs (Mpc), is the distance from the object being measured to the observer. The distance used is the distance between where the observer is at the moment of observation and where the object was when it emitted its light.

D. Alternate methods to calculate the Hubble constant.

1. Calculation method using calibrated angle

The angle θ can be calibrated so that trigonometric functions can read out directly in velocity. The calibration is based on the fact that the distance of travel in the x axis that occurs during a light second of travel in the y direction calculates velocity.

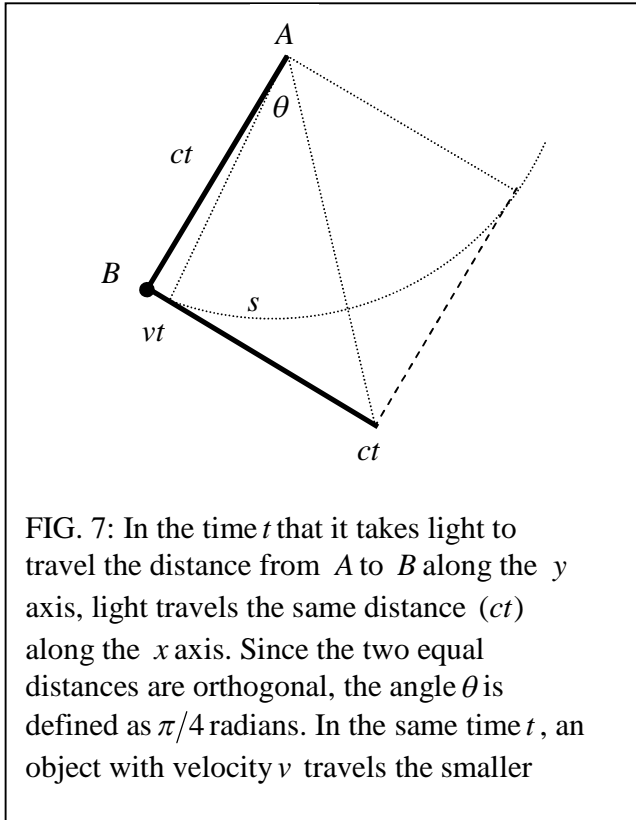
As can be seen in FIG. 7, in the time t it takes light to travel the distance from A to B along the y axis, light travels the same distance (ct) along the x axis. Since the two equal distances are orthogonal, the subtended angle θ , is defined as $\pi/4$ radians.

$$\theta = \left(\pi/4 \frac{ct}{ct} \right). \quad (12)$$

Since the time t is a constant, it can be factored out to show the equation in terms of velocity. In the same time t , an object with velocity v travels the smaller distance vt and subtends a smaller angle.

$$\theta = \left(\pi/4 \frac{v}{c} \right). \quad (13)$$

This calibration assumes that velocity is linear with the angle. As can be seen in FIG. 7, this is not a valid assumption; however, for the very low velocities ($\leq 11.34 \text{ km/s}$) used in this paper, it can also be seen that the error is insignificant. [36]



Substituting the calibrated angle for θ then provides the difference in distance in terms of km/s . The distance x can be expressed as v and the distance y can be expressed as c .

$$\Delta ct/s = \left[2ct \sin\left(\pi/4 \frac{v}{2c}\right) \right] - \left[ct \sin\left(\pi/4 \frac{v}{c}\right) \right] \quad (14)$$

The angle in radians per velocity of 1 km/s is given by:

pi/4	v	c	θ
(radians)	(km/s)	(km/s)	radians * (km/s)
0.785398163	1	299792.458	2.619806277E-06

Table 4: Value of angle for a velocity of 1 km/s

Once the angle is calculated, the recession velocity can be calculated for 1 light second with the following values from the definition of the parsec: [37]

$$v = 1km / s$$

Angle θ is from Table 6

Wavefront travel distance $ct = 299,792.458km$ (1light second)

Perspective	Function	Values($km/s/ls$)
Common	$2ct \sin \theta/2$	0.785398163397224
Individual	$ct \sin \theta$	0.785398163396550
	v_a	0.0000000000000674

Table 5. The subtraction yield a difference of $v_a = 6.74 \times 10^{-13} km/s/ls$

Since the difference is cumulative, to determine the recession velocity at one mega parsec, this velocity that was calculated for one light second must be multiplied by the number of light seconds in a mega parsec,

$$v_a = (6.74 \times 10^{-13})(1.03 \times 10^{14}). \quad (15)$$

This calculation yields the artifact velocity per megaparsec

$$v_a = 69.4 km/s/Mpc. \quad (16)$$

2. Calculation method using redshift

The Hubble constant is the recession velocity expressed per megaparsec and the recession velocity is the product of the redshift and the speed of light. [37][38] If the parsec ($pc = AU/\tan \theta$) is considered the distance of the emitted wavelength λ_{emit} , then the wavelength actually measured by the Earth observer ($pc = AU/\sin \theta$) becomes the observed wavelength λ_{obs} . In both cases, $\theta =$ one arcsecond and AU is the distance between the Sun and the Earth. [39]

As can be seen in Table 6, the recession velocity artifact v_a for one parsec is the product of the redshift z and the speed of light c . A calibration factor of 19.7 is needed for correct velocity. This same factor is seen in the comparison of recession velocity and redshift in Section V, where it yields a ratio of 1 c velocity to 1.46 redshift. It is analogous to the distance modulus. [40]

$\lambda_{emit} = AU/\tan \theta$	$\lambda_{obs} = AU/\sin \theta$	$z = (\lambda_{obs} - \lambda_{emit})/\lambda_{emit}$	$v_a = cz$	$19.68 * v_a$
(km)	(km)		(km/s)	(km/s)
30,856,775,814,642.4	30,856,775,815,005.0	1.1752155E-11	3.523E-06	6.93-05

Table 6: The recession velocity artifact v_a is calculated for a parsec. A calibration factor of 19.68 is needed for correct velocity.

Multiplying the value of the recession velocity for one parsec by a factor of a million expresses the calibrated artifact velocity per megaparsec, which is the form of the Hubble constant

$$v_a = 69.3 \text{ km/s/Mpc} \quad (17)$$

E. Comparison of results with different methods

On 3 October 2012, it was announced that the Hubble constant value measured by NASA's Spitzer Space Telescope was 74.3 km/s/Mpc. On 20 December 2012, it was announced that the Hubble constant value measured by NASA's Wilkinson Microwave Anisotropy Probe (WMAP) was $70 \pm 2 \text{ km/s/Mpc}$. On 21 March 2013, it was announced that the Hubble constant value measured by ESA's Planck Mission was $67.80 \pm 0.77 \text{ km/s/Mpc}$ [41]

FIG. 8 shows the wide range of values that have this far been determined for the Hubble constant by different methods at different times. [42]

NASA has studied the results from the various methods and has determined the best estimate of the Hubble constant based on all information to be $69.3 \pm 0.8 \text{ km/s/Mpc}$. In a quote from an article updated on 21 December 2012 [43], NASA explains how their value could be derived from a combination of different methods:]

“However, if we do not make an assumption of flatness, we can combine WMAP data with other cosmological data to get 69.3 km/sec/Mpc (give or take 0.8 km/sec/Mpc), a 1% solution that combines different kinds of measurements. After noting that independent observations give consistent results, it is reasonable to combine information to get the best estimate of parameters”

As a reminder, the three results derived for the velocity artifact v_a were 70, 69.4 and 69.3 km/s/Mpc. Each of these three calculated results is within the error limits set by NASA. The 69.3 km/s/Mpc value exactly matches NASA's nominal value.

III .EXPLANATION OF RECESSION AND REDSHIFT VELOCITY ARTIFACTS

A. Recession velocity artifact.

FIG. 9 uses trigonometry as a tool to better understand the relationship between distances in the observer-centered perspective as seen by an observer on Earth. In taxicab geometry, the distance from the Sun and the Earth to the star is defined as one parsec. This makes the wavefront travel time t from the star to both objects equal. For simplicity, the wavelength of the light is set to be one parsec so that time t equals the time interval T .

Because the actual wave travel distance is longer to the Earth (cT) than a parsec, but is measured with the parsec wave travel time ($T \cos \theta$), the Earth observer measures a longer wavelength λ_{obs} than the wavelength emitted from the source λ_{emit} .

Since light travels at c , the extra distance measured by the Earth observer must be accounted for. At present, the distance is explained by cosmic expansion of the universe. However, as can be seen, the distance is actually an artifact of observation ($v_a t$)

Although the Earth observer perceives the longer wavelength as cT , other factors make it clear that something is wrong. First, the wavelength gets longer with distance (redshift) and second, the observed wavelengths at the longer distances do not agree with the wavelengths emitted by the stars, as expected by spectroscopy. [44]

Therefore, the Earth observer defines the observed wavelength cT in terms of the actual speed of light $ct \cos \theta$ plus $v_a T$ which is the distance believed to be caused by the cosmic expansion.

$$cT = cT \cos \theta + v_a T . \quad (18)$$

Dividing both sides of the equation by the time interval T compares the relationship in terms of velocity instead of distance.

$$c = c \cos \theta + v_a . \quad (19)$$

Solving for the artifact velocity

$$v_a = c - c \cos \theta . \quad (20)$$

The speed of light c can be factored

$$v_a = c(1 - \cos \theta) . \quad (21)$$

Note: This equation is the same as Equation 6, which was derived directly from the time and distance factors.

Dividing by c on both sides of the equation

$$\frac{v_a}{c} = 1 - \cos \theta . \quad (22)$$

As can be seen, the artifact velocity function v_a is sinusoidal. When it is simply used in the Hubble equation, it produces a linear increase in wavelength with distance (recession velocity) for a relatively short distance ($<1c$).[45]

B. Redshift velocity artifact

1. Calculation of redshift artifact

When the data is normalized, it causes the radial distance to remain constant while the angle increases. It is this effect of normalization that causes the sinusoidal shapes that are observed in the z function.

The redshift velocity artifact z_a will be demonstrated to be the ratio of the apparent change in wavelength ($\lambda_o - \lambda_e$) due to the difference in frames of reference with the wavelength observed in the Earth's frame of reference λ_e . As a ratio, the nanometer units cancel. As will also be demonstrated, the normalization makes redshift into a function of the cosine of the angle θ (*adj/hyp*) rather than just a function of the distance (*adj*).

With normalization, the radial difference between the two wavelengths does not increase with distance. Instead, the radial distance remains constant, it is the transverse distance (and the angle) that increases.

As can be seen in FIG 9, in the source-centered perspective, the radial distance cT to the Earth is longer than the radial distance to the Sun. The distance from the star to the Earth is a single wavelength cT . Since the distance to the Sun is shorter, only part of the wavelength $cT \cos \theta$ is seen by an observer there.

In the observer-centered perspective, the radial distance y is the same to both the Sun and the Earth position. Since the observer-centered perspective is used in astronomy, it must be explained why the wavelength is observed to be longer when observed on Earth. The current justification for the longer distance is that it is caused by the expansion of the universe.

The redshift velocity artifact z_a is a measure of the observed wavelength increase caused by the difference in observer perspectives. [46]

$$z_a = \frac{\lambda_o - \lambda_e}{\lambda_e} \quad [23]$$

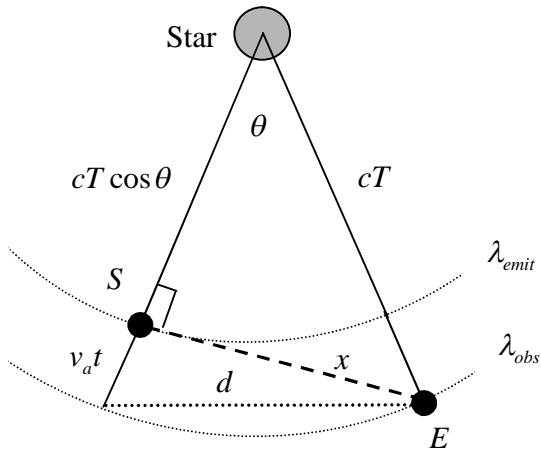


FIG.9. Time is measured as the wavelength interval T ; the distance to the star is made one wavelength to help in understanding. Each point on the x baseline shares the same time interval T but has a longer wavefront travel distance cT , causing each observer on the x axis (except on the Sun) to observe a redshift. The artifact distance $v_a T$ is currently explained by cosmic expansion of space.

Redshift is calculated by determining the difference in distance between the wavelength observed in the Earth's frame of reference $\lambda_o = cT$ and the wavelength observed in the Sun's frame of reference $\lambda_e = c \cos \theta T$, and then normalizing that difference to the Earth's frame of reference by dividing through by $c \cos \theta T$.

$$z_a = \frac{cT - c \cos \theta T}{c \cos \theta T}$$

The equation can be divided through and separated.

$$z_a = \frac{cT}{c \cos \theta T} - \frac{c \cos \theta T}{c \cos \theta T}$$

The ratio of emitted wavelengths is simplified to 1

$$z_a = \frac{cT}{c \cos \theta T} - 1$$

Adding 1 to both sides puts the result in terms of the ratio of the observed to the emitted wavelengths

$$z_a + 1 = \frac{cT}{c \cos \theta T} \quad (24)$$

cT is factored on the right side of the equation to simplify the result.

$$1 + z_a = \frac{1}{\cos \theta} \quad (25)$$

Subtracting 1 from both sides of the equations gives the result in terms of the redshift velocity artifact.

$$z_a = \frac{1}{\cos \theta} - 1 \quad (26)$$

2. Redshift artifact derived in the special theory of relativity.

As discussed previously, actual redshift requires a positive radial displacement (velocity) between the light source and the observer. By definition, travel in the transverse direction (without a change in radius) generates zero radial velocity and cannot cause an actual redshift.

However, as has been demonstrated in the previous section, a redshift artifact occurs because of radial displacement contained within the transverse distance in the taxicab geometry. This redshift component in transverse distance was verified experimentally in 1938 by Herbert E. Ives and G.R. Stilwell. It is commonly known as the Transverse Doppler Effect (TDE). [47]

This redshift artifact (defined as an increase in wavelength without radial motion) was first predicted in by Einstein in 1905. [48]As explained within special relativity, the Lorentz factor is dependent only on the magnitude (speed) of motion and is not affected by its vector direction. The relativistic correction made to the Doppler Effect equation therefore includes effects from both radial and transverse motion.

The classical Doppler formula is dependent solely on radial displacement (line-of-sight movement) to or from the light source. In the full form relativistic Doppler equation, θ is the angle between the direction of relative motion and the direction of emission in the observer's frame of reference (an angle of zero is directly away from the observer). [48]

The full form for the relativistic Doppler Effect is:

$$1+z = \frac{1+v \cos \theta / c}{\sqrt{1-v^2/c^2}} \quad [27]$$

In the special case that the light approaches at right angles ($\theta = 90^\circ$) to the direction of relative motion in the observer's frame, $\cos \theta$ becomes zero so the numerator of the equation becomes one. This means even though all movement is transverse and therefore theoretically cannot generate actual radial velocity, a redshift artifact with the equation

$$1+z_a = \frac{1}{\sqrt{1-\frac{v^2}{c^2}}} \quad (28)$$

is observed.. Note: Even when the source is moving towards the observer, if there is a transverse component to the motion then there is some speed at which the dilation just cancels the expected blueshift and at higher speed the approaching source will be redshifted. [49]

The variable in the TDE equation can be converted from velocity to distance to allow a comparison with the equation derived from the difference between the two perspective times.

First, since the ratio of v^2 to c^2 is dimensionless, it can be rewritten in terms of distance instead of speed by multiplying both the numerator and denominator by time t .

$$1+z = \frac{1}{\sqrt{1-\frac{(vt)^2}{(ct)^2}}} \quad (29)$$

Next, the magnitude of x can be substituted for vt which is allowed in the usual case of velocity where $t = \text{one second}$.

$$1+z = \frac{1}{\sqrt{1-\frac{x^2}{(ct)^2}}} \quad (30)$$

3. Comparison of equations of the two theories for the redshift artifact

The equation for the redshift artifact z_a which was derived from the *difference in perspectives* was seen previously as Equation 17.

$$1 + z_a = \frac{1}{\cos \theta} \quad [31]$$

The following equation for the redshift artifact z_a was derived from special relativity (modified to have the variable as distance instead of velocity)

$$1 + z_a = \frac{1}{\sqrt{1 - \frac{x^2}{(ct)^2}}} \quad [32]$$

A comparison between the two equations can be performed. As was seen previously in FIG.9, the distance ct can be expressed in terms of x and $ct \cos \theta$ by means of the Pythagorean Theorem.

$$((ct)^2 = (ct \cos \theta)^2 + x^2. \quad (33)$$

The equation can then put in terms of $ct \cos \theta$ by subtracting x from both sides.

$$((ct \cos \theta)^2 = (ct)^2 - x^2. \quad (34)$$

The equation can then be normalized to the Earth's frame of reference by dividing through both sides of the equation with $(ct)^2$. This process cancels the equal functions and creates dimensionless units.

$$\frac{(ct \cos \theta)^2}{(ct)^2} = \frac{(ct)^2}{(ct)^2} - \frac{x^2}{(ct)^2} \quad (35)$$

Taking the square root of both sides and simplifying provides the ratio of the wavefront distances from the two frames of reference.

$$\frac{c \cos \theta t}{ct} = \sqrt{1 - \frac{x^2}{(ct)^2}}. \quad (36)$$

The common term ct on the left side can be canceled,

$$\cos \theta = \sqrt{1 - \frac{x^2}{(ct)^2}}. \quad (37)$$

The unit exchange between velocity and position can be done in either direction without affecting the magnitude since the units cancel in the ratio. For instance, the term $\cos \theta$ can be expressed in terms of velocity instead of position. First, the position x^2 is expressed as velocity times time $(vt)^2$

$$\cos \theta = \sqrt{1 - \frac{(vt)^2}{(ct)^2}} \quad (38)$$

Then the time t can be cancelled in the ratio to present the distance as velocity in order to directly compare to the apparent redshift equation caused by different perspectives.

$$\cos \theta = \sqrt{1 - \frac{v^2}{c^2}} \quad (39)$$

Therefore, the following relationship can be made:

$$1 + z_a = \frac{1}{\cos \theta} = \frac{1}{\sqrt{1 - \frac{v^2}{c^2}}} \quad (40)$$

As can be seen, the equation derived for the apparent redshift from the difference between the observer-centered and source-centered perspectives is equal to the TDE equation for the redshift artifact. This agreement with the TDE equation gives strong experimental evidence to support the hypothesis that the observed redshift is an artifact of observation caused by a difference in perspective of the observer rather caused by physical cosmic expansion.

IV. EFFECT OF DISTANCE ON THE MAGNITUDE OF THE ARTIFACT

To maintain the magnitude of the parsec distance unit as determined by the equation $y = x/\tan \theta$ as distance to the star increases, the angle must stay the same. However, by reducing the angle, distance to nearby stars can be measured using the fact that one arc second equals one parsec. As an example, when the angle is reduced to one half of an arc second, the distance is two parsecs.

As can be seen in FIG.10, as the angle decreases, the error per unit also decreases. This may confuse understanding of cumulative effects of the parsec unit. If the parallax method were used for all distance measurements, the error would, in deed, diminish with distance, not accumulate, but the technique has been limited to a relatively short range. [50]

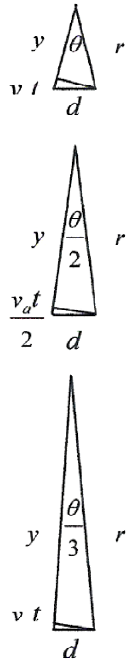


FIG. 10. The parallax method can be used to determine distance to nearby stars. Note: the angle reduces as distance increases which also reduces the error Δr proportionally.

All longer range techniques, which are included in what is known as the distance ladder, are based on the parsec unit with its *full* angle of one arc second. As can be seen in FIG. 11, the error is the identical for each parsec unit and accumulates with increasing distance. [51]

When the angle θ is held at 1 arc second, then as ct increases to 1 megaparsec, d will increase and v_a will equal 70 km/s . This linear relationship continues for multiple parsecs according to Hubble's law. [52]

The increase in the velocity artifact is perceived in two ways as can be seen in FIG. 10. On the left of the figure, the small difference in Δr for each individual parsec is added to a total. . On the right of the figure, Δr is shown totaled in one similar triangle scaled with a longer radius and baseline. [53]

The sum of the individual multiple parsecs on the left provide the same apparent velocity as the increased scaled distances on the right. The effect is the same as if the distances had been increased proportionally when setting the parsec's radial magnitude.

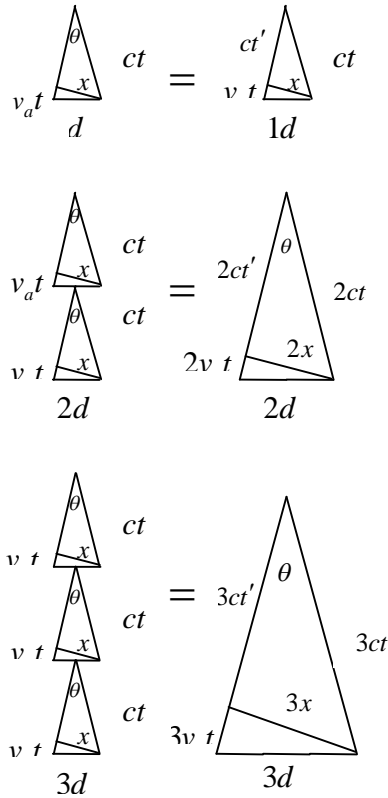


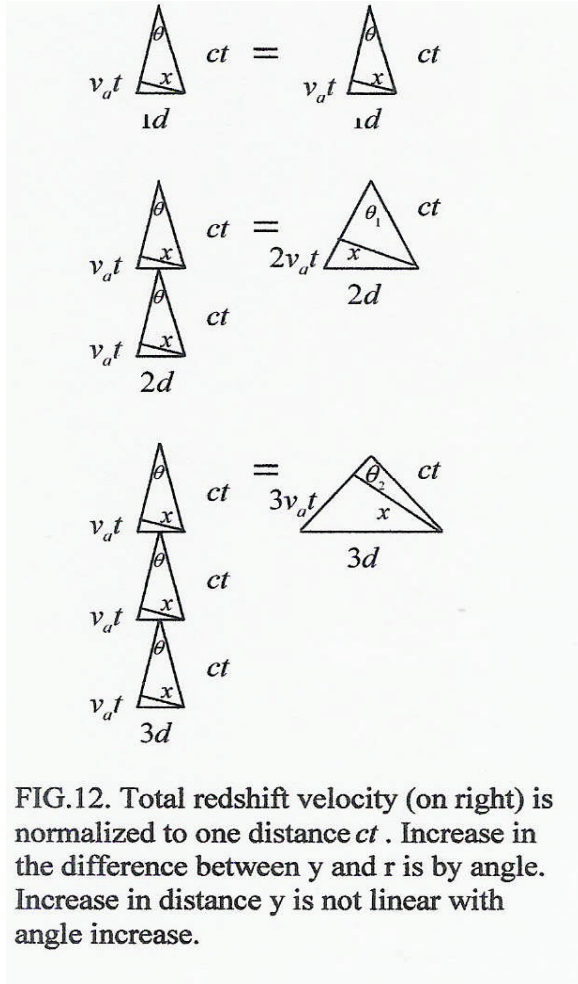
FIG.11. Cumulative error in source-centered perspective. Because similar triangles can be scaled, the sum of $v_a t$ in individual multiple parsec units equals $v_a t$ in one large distance. The relationship is linear between the sides.

The calculation of redshift normalizes the difference between the observed and emitted wavelengths to the vector magnitude of the emitted wavelength. In trigonometric terms, the normalizing process divides the wavelength difference between the observed wavelength and the emitted wavelength ($cT - c \cos \theta T$) by the emitted wavelength $c \cos T$. [54]

The cumulative increase in redshift, observed in FIG 12, is non-linear, specifically sinusoidal. This compares to the cumulative increase in recession velocity which is linear in FIG.11. There is nothing inherent in the normalization process to cause a sinusoidal function; it occurs because the factor between the observed and emitted wavelength is $\cos \theta$. [55]

As will be seen, this prediction is proven by the observed sinusoidal shape of the general relativity relationship between velocity and redshift.

The total of the individual parsecs is on the left side with the total $v_a t$ for the whole distance on the right side. In this case, the relationship between the two sides is non-linear with distance.



V. GENERAL RELATVITY MODELS

Both the non-linear relationship between velocity and redshift and the non-linear relationship between distance and the scale factor are currently explained by the Friedmann–Robertson–Walker (FRW) metric as due to the physical effects of expansion. The FRW metric is an *ad hoc* solution to the extent that the factors of the metric are selected based on fitting observations of the cosmos. [56]

It will be demonstrated that these non-linear relationships are due to the sinusoidal nature of the artifact caused by the difference between the source-centered and observer-centered perspectives.

A. Velocity vs. redshift

FIG. 13 shows the accepted curve shapes for the supposedly linear relationship of recession velocity divided by c and the FRW general relativity model for redshift velocity. The special relativity curve is not generally accepted. [57]

Note the wide variation (gray area) in the general relativity models. The actual line represents the observationally selected FRW model $\Omega_M, \Omega_\Lambda (0.3, 0.7)$ which is sinusoidal and asymptotic to velocities of $0c$ and just over $3c$. In this model, a redshift value of 1.46 correlates with a recession velocity of $1c$. [58]

The function that was derived for the red shift artifact in this paper is $z_a = 1/\cos\theta - 1$. The function has a domain of $\pi/2$ radians and a range of infinity. The red shift values and corresponding velocity values for this domain are shown in Table 4. They are calibrated to fit this FRW model by a factor of 20, as will be seen. [59]

The function for the recession velocity artifact divided by the speed of light is $v_a/c = 1 - \cos\theta$. It has the same domain and range as the redshift artifact..

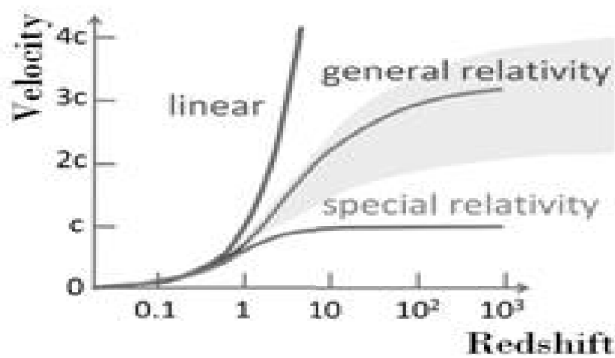


FIG. 13 The general relativity line is the observationally selected FRW model $\Omega_M, \Omega_\Lambda (0.3, 0.7)$, which is currently believed to be due to the interaction of matter, energy, and the cosmological constant. The linear line is the recession velocity divided by c . The special relativity line is not appropriate in this context.

Compare the general relativity curve in FIG. 13 with the $1/\cos\theta - 1$ curve in FIG. 14. The curve matches closely follows the FRW general relativity graph of velocity vs. redshift after calibration. It is sinusoidal and is asymptotic to both zero and just above a velocity of $3c$. A velocity of $1c$ gives a redshift of 1.453, which nearly matches the expected redshift of 1.46. Further adjustments can be made in the multiplication factors if required.

Compare the linear curve in FIG. 13 with the calibrated v_a/c curve in FIG.14. In both figures, the linear curve very closely approximates the FRW curve until the velocity approaches 1 where the two curves quickly diverge.

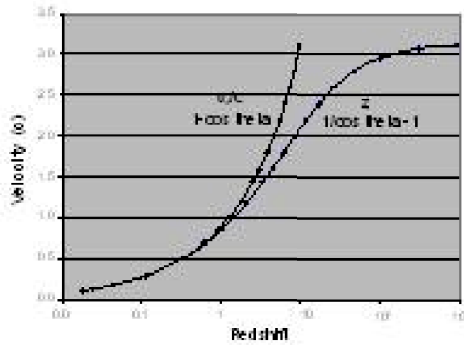


FIG.14: Data from Table 4 is displayed showing the calibrated function $1/\cos\theta - 1$ for redshift velocity z and the calibrated function $1 - \cos\theta$ for recession velocity divided by the speed of light.

In Table 7, the first column is the angle θ in radians ranging in small increments from 0.02 to close to 2π radians. The second column is the linear velocity numbers which are simply the value of the angle θ in radians multiplied by a factor of 2 in order to approximate the same curve the result of the function with the corresponding angle. The third column is the redshift z_a function multiplied by a factor of 9.68 to provide a calculation to match the FRW curve in FIG. 11. The fourth column is the v_a/c function which is also multiplied by a factor of 9.68 to match the observed values.

As seen previously, the factor of 9.68 was also used to calculate the Hubble constant from redshift. With this factor, the Hubble constant exactly equaled NASA's value. The factor is a calibration which is analogous to the distance modulus, which is discussed in footnote 40.

Angle θ	Velocity c	Redshift z_a	Recession v_a/c
	$\theta * 2$	$(1/\cos \theta - 1) * 9.68$	$(1 - \cos \theta) * 9.68$
Radians	km/s		km/s
0.02	0.04	0.00	0.002
0.03	0.06	0.00	0.004
0.04	0.08	0.01	0.008
0.05	0.10	0.01	0.012
0.06	0.12	0.02	0.018
0.07	0.14	0.02	0.024
0.09	0.18	0.04	0.040
0.15	0.30	0.11	0.112
0.26	0.51	0.35	0.336
0.35	0.69	0.65	0.606
0.43	0.85	1.00	0.910
0.51	1.00	1.46	1.273
0.60	1.18	2.12	1.747
0.72	1.42	3.33	2.500
0.80	1.58	4.35	3.033
0.90	1.77	6.09	3.784
1.00	1.97	8.51	4.597
1.10	2.17	12.05	5.464
1.20	2.36	17.60	6.376
1.30	2.56	27.38	7.325
1.40	2.76	48.83	8.300
1.48	2.92	100.29	9.093
1.54	3.03	314.77	9.692
1.56	3.07	916.26	9.892
1.57	3.09	12547.66	9.992

The scale factor artifact $a(t)_a$ was derived from the sinusoidal relationship of radial distance in the source-centered perspective and the observer-centered perspective. Since radial distance can be represented by ct , radial distance to an object can represent elapsed time from that object. The scale factor can be interpreted as a measure of expansion.

According to the FRW metric, if at the present time light is received from a distant object with a redshift of z , then the scale factor at the time the object originally emitted that light is given by the equation. [60]

$$a(t) = \frac{1}{1+z} \quad [41]$$

It was demonstrated previously that $1+z = 1/\cos\theta$, so the substitution can be made in the equation.

$$a(t)_a = \cos\theta \quad [42]$$

It can be seen in FIG. 15, that the function for the apparent scale factor $a(t)_a = \cos\theta$ has a domain of $\pi/2$ radians and a range of infinity. The scale factor values and corresponding wavelength values for this domain are shown in Table 5. Note: The perturbation mode goes with the scale factor and so is a 45 degree line on this plot. [61]

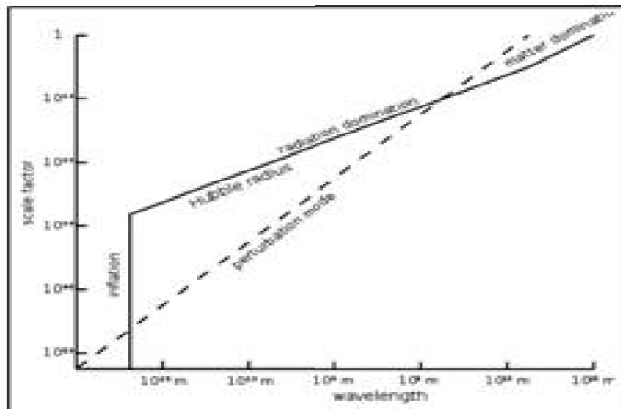


FIG.15 The accepted explanation of the Hubble radius expansion includes a physical inflation era of extremely rapid growth. The expansion is seen in this log-log plot of the normalized scale factor of the universe vs. wavelength.

Just as the curve in FIG. 15 can be changed by different variables in the FRW model to create the desired fit to velocity, these values can also be changed in this model. However, because of the great range of the values, no attempt was made in Excel to be quantitative. This is purely a qualitative comparison of curve shapes and intercepts.

Note that the slope change in FIG. 15 is very acute as compared to the slope change in FIG. 16. The appearance of the change depends on the scale of the data. In a log-log plot, the smaller values are overemphasized compared to the larger values. If the change in FIG.15 is expanded, a more gradual change will be seen.

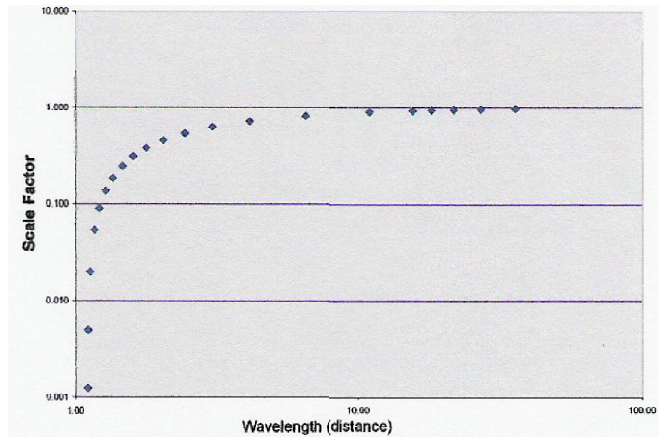


FIG.16 The log-log graph of data from Table 2 shows that the shape of the function $1 - \cos \theta$ fits the accepted graph of the expansion of the Hubble radius, plotting the scale factor vs. distance. Note the very high slope portion of the curve which matches the shape of the inflationary era followed by the slow change in slope. Also note the intersection with the x axis. No attempt was made to calibrate the function; this is a qualitative comparison only.

Although the scale factor is equal to $\cos \theta$, $1 - \cos \theta$ was plotted against the wavelength. This was because the observer origin was moved from zero to one so that the convention that the value of the scale factor at the present time is one could be maintained

Angle θ	$1 - \cos \theta$	$\Delta \lambda$
0.05	0.001	1.10
0.1	0.005	1.11
0.2	0.020	1.12
0.33	0.054	1.16
0.43	0.091	1.21
0.53	0.137	1.27
0.62	0.186	1.35
0.72	0.248	1.46
0.81	0.311	1.60
0.9	0.378	1.77
1	0.460	2.04
1.1	0.546	2.43
1.2	0.638	3.04
1.3	0.733	4.11
1.4	0.830	6.47
1.47	0.899	10.93
1.5	0.929	15.55

1.51	0.939	18.10
1.52	0.949	21.66
1.53	0.959	26.97
1.54	0.969	35.72

Table 8: The scale factor function was made to be $1 - \cos \theta$ in order to “look back” from one.

As can be seen in FIG. 14, the $1 - \cos \theta$ function exhibits the same characteristics as the Friedmann–Robertson–Walker model of the scale factor showing the effect of inflation in the Hubble radius expansion.

VI. PROOFS

A. Dark Energy

1. *Background*

As previously explained in Section II A, the difference between the source-centered perspective and the observer-centered perspective causes the Earth observer to perceive a longer parsec having the same wave front travel time as the defined parsec unit. This combination of longer perceived distance with the same perceived time creates a velocity artifact that manifests as an apparent redshift that increases with distance.

Since redshift is currently interpreted as the result of actual physical cosmic expansion, it is logically for astronomers to use redshift to determine distance to stars and galaxies. The first redshift-distance relationship was the Hubble Law, which used multiples of recession velocity. [62] Later, a new relationship, known as the Friedman-Robertson-Walker (FRW) metric, was developed using general relativity with comoving distance to extend the useful range. [63]

As will be demonstrated, it is the same longer perceived length of the parsec that causes the redshift artifact, which also causes the redshift distance to be shorter than expected.

As is well-known, but sometimes overlooked, distance is actually measured as a count of units. Therefore, a longer unit reduces the numerical count of the units which makes the distance appear shorter. For example, if distance were accidentally measured in meters instead of yards, each unit would be about 3 inches too long. For every 12 yards measured with the long (meter-sized) unit, the distance will be shorter by 1 yard ($36in = 12 \times 3in$), which shows that the error is cumulative with distance.

It is important to note that the error in distance in the example could be corrected if the sum of the shortfall accumulated-to-date were to be added back to the individual distance

measurements at a rate of 3 inches per yard. As will be seen, this same add-back correction is also possible with redshift distance.

2. Determination and correction of redshift distance shortfall

Since the longer perceived parsec is both the cause of the redshift and the cause of the redshift distance shortfall, the magnitude of both effects is identical. Therefore, the extra distance of the parsec can be added back to the redshift distance for correction. The extra distance of the parsec is the difference in distance between the source-centered and observer-centered perspectives, which is given by the equation

$$2r \sin \theta / 2 - r \sin \theta . \quad [43]$$

As was seen in the example with the meter and the yard measurement s , a correction for the shorter distance can be made by adding the total distance error back to the redshift artifact. The redshift artifact was defined in Equation 26 as $1/\cos \theta - 1$. Therefore, the corrected redshift distance is the sum of the original redshift and the shortfall error.

$$z_{corr} = \left(\frac{1}{\cos \theta} - 1 \right) + (2r \sin \theta / 2 - r \sin \theta) \quad [44]$$

The angle θ_{cal} used to determine the shortfall error calculation is calibrated to fit the individual redshift readings with the following calculation.

$$\theta_{cal} = z_a \pi / 2 \quad [45]$$

This concept of correcting the redshift shortfall will be tested by populating the redshift and distance correction equations with artificial values and then proved by using actual observed redshift values.

For the test of the concept, table 9 is populated with a linear progression of numbers in the Angle column. They can be calibrated to represent any linear function. All other positions in the table are calculated.

Angle	Calculated z	Cal. angle	Shortfall error	Corrected z
θ	$z_a = 1/\cos \theta - 1$	$\theta_{cal} = z_a \pi / 2$	$2r \sin \theta_{cal} / 2 - r \sin \theta_{cal}$	$z_{corr} = z_a + error$
0.200	0.020	0.031948	0.000	0.020
0.300	0.047	0.073437	0.000	0.047
0.400	0.086	0.134624	0.000	0.086
0.500	0.139	0.219117	0.001	0.141
0.600	0.212	0.332425	0.005	0.216
0.723	0.333	0.52372	0.018	0.351
0.800	0.435	0.683806	0.039	0.474

0.900	0.609	0.956184	0.103	0.712
1.000	0.851	1.336458	0.267	1.117
1.100	1.205	1.892188	0.673	1.878
1.200	1.760	2.764136	1.596	3.356
1.260	2.270	3.565598	2.367	4.637
1.300	2.738	4.301365	2.590	5.328

Table 9. The table contains the data displayed in FIG.16.

FIG. 16 shows the redshift function $(1/\cos\theta - 1)$ with its characteristic sinusoid curve and the corrected redshift with the added shortfall distance function $(2r \sin\theta/2 - r \sin\theta)$. The functions are both populated with data from Table 9.

Note that the individual redshift and corrected redshift values are on the same level on the graph. The effect of the correction can be seen to be cumulative. It is important to note that the corrected readings above the redshift value of 4.6 become increasingly non-linear, even retrograde, then again become linear.

With the test of the concept complete, the next step is to prove the concept with real redshift data. For this to be possible, the distance shortfall must be discovered. For the shortfall to be discovered the distance to the star or galaxy has to become large enough to make the cumulative shortfall measurable and an independent method has to be available to accurately measure the distance for comparison.

Luckily, the type 1a supernovae already provide both of the required factors. They are very far away and they are standard candles. Again luckily, the redshift shortfall has already been discovered. Therefore, the proof of the correction on real redshift data can begin.

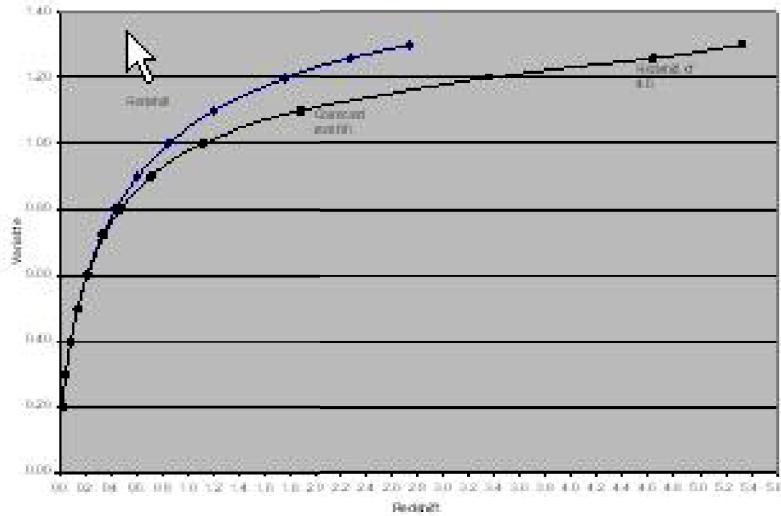


FIG.16: The redshift curve is the equation $(1/\cos\theta - 1)$ and the corrected redshift curve is the same equation plus the equation $(2r \sin\theta/2 - r \sin\theta)$. The correction adds back the distance that the artifact lost, making the redshift-distance relationship accurate up to a redshift of 4.6. The concept is logical and works well; what is needed is proof on real redshift data.

3. Discovery of the redshift distance shortfall

Riess et al in 1998 found that a type of supernovae (SNe 1a) were dimmer than expected based on their distance. [64] The best explanation was that the supernovae were actually further away than the FRW redshift-distance calculations had predicted. [65] It was theorized that the extra distance was caused by a speedup in the expansion of the universe caused by an unrecognized energy, which, because it was undetectable, came to be known as dark energy. [66]

In a study where the standardized peak magnitudes of a total of sixteen high redshift and 34 low redshift Type Ia supernovae were plotted against redshift velocity, Riess et al (1998) observed that the observed luminosity distance of the low-redshift Type Ia supernovae met expected values, but the high-redshift supernovae luminosity distance was less than expected values. [67]

The observed flux of a SNe type Ia supernova depends on its intrinsic luminosity, its distance from the observer and the amount of astrophysical absorbing material in the light path. (Later experiments would rule out light absorption by dust or other astrophysical debris as a cause of the dimness. [68] Therefore, an incorrect distance could account for the lower observed flux of the supernovae.

The distance from the observer to the supernovae can be determined in two ways:

- i. Using the FRW redshift-distance method

The luminosity distance D_L in the Friedmann-Robertson-Walker cosmologies was calculated for each redshift with the formula

$$D_L = cH_0^{-1}(1+z)|\Omega_k|^{-1/2} \sin n \left\langle \int_0^z \left[(1+z)^2 (1+\Omega_M z) - z(2+z)\Omega_\Lambda \right]^{-1/2} dz \right\rangle \quad (46)$$

where H_0 is the Hubble constant, Ω_m is the mass density, and Ω_Λ is the cosmological constant. $\Omega_K = 1 - \Omega_M - \Omega_\Lambda$ and $\sin n$ is \sinh for $\Omega_K \geq 0$ and \sin for $\Omega_K \leq 0$. [69]

- ii. Using intrinsic luminosity method

The luminosity distance D_L was calculated from SNe Ia light data with the formula,

$$D_L = \left(\frac{L}{4\pi F} \right)^{-2}, \quad (47)$$

where L and F are the SNe Ia intrinsic luminosity and observed flux, respectively. [70]

D_L for both methods is calibrated in units of megaparsecs. The distance modulus is calculated by [71]

$$u_p = 5 \log D_L + 25. \quad (48)$$

From the point of view that the problem was distance and not luminosity, the intrinsic luminosity distances of the high-redshift SNe Ia were calculated to be, on average, 10% to 15% greater than the FRW redshift distances. [72]

It was decided that the most likely reason that the redshift distances were too short was because they did not include the acceleration of the cosmic expansion fueled by positive vacuum energy density. A positive cosmological constant was seen as the most plausible explanation. [73] However, in what Riess and Turner (2004) later said has been called the worst embarrassment in all of theoretical physics, the energy density values associated with quantum vacuum were measured to be a minimum of 55 orders of magnitude higher than predicted. [74]

With the observationally selected values for the FRW constants plus the *ad hoc* value of the cosmological constant, the redshift distance has been made to equal the intrinsic distance of the supernovae. However, to date, there is no physical explanation for the source of the dark energy that is claimed to constitute 68% of the universe. [75]

4. Application of the redshift distance correction equation

As can be seen in the last section, the sole evidence for dark energy is the unexplained shortfall in redshift distance. As proposed, the shortfall in the redshift distance is instead due to the effect of the longer parsec magnitude perceived by the Earth observer, which in turn is caused by the observer-centered perspective as was earlier described.

To correct for the artifact error, the distance difference between the two perspectives is determined, then added to the observed redshift distance.

When data is presented in the form of velocity v , as it is the Hubble constant and Pioneer Anomaly applications, the observed velocity artifact v_a had to be divided by c to translate into redshift velocity

$$\theta = \left(\frac{\pi}{4}\right)\left(\frac{v_a}{c}\right) \quad (49)$$

However, the data in this application is provided is in the form of observed redshift artifact z_a , not velocity; therefore the formula to determine the angle is modified to eliminate the division by c . Also, because the domain of the redshift function is $\pi/2$, the angle is changed to $\pi/2$.

$$\theta = \left(\frac{\pi}{2}\right)(z_a) \quad (50)$$

The calculation of the distance difference Δs using the calibrated angle θ is as follows:

$$\Delta s = 2r \sin\left(\frac{\theta}{2}\right) - r \sin \theta \quad (51)$$

The next step is to calibrate the angle by multiplying it by the observed redshift value. The calibrated angle is used in the calculation of the source-centered distance d and the observer-centered distance x . The difference $(d - x)$ is then used as a correction for the redshift. z_c . The corrected redshift z_c is shown to be equal to MB, the stretch luminosity-corrected B-band peak magnitude.

Observed redshift z_a	Calibrated angle θ	Source-centered distance (d)	Observer-centered distance (x)	Distance shortfall Δs	Corrected redshift z_c
z_a	$(\pi/2)z_a$	$2r \sin \theta/2$	$r \sin \theta$	$d - x$	$z_a + \Delta s$

Table 10: Headings for data tables (not including MB) showing the calculations made for each heading, starting with the observed redshift reading z_a .

5. Data tables

Data from the previously-mentioned published studies are found in Table 11-15.

Explanation:

- Col 1: (SN) IAU name assigned to SCP supernova (from source)
- Col. 2: (z_a) Observer-centered redshift velocity Z of supernova or host galaxy (from source)
- Col. 3: (θ) Angle θ - calculated as $\pi/2 * \text{redshift velocity } z$ -Note: $z = v/c$
- Col. 4: ($2r \sin \theta/2$) Redshift velocity z based on source-centered distance
- Col. 5: ($r \sin \theta$) Redshift velocity z based on observer-centered distance
- Col. 6 (Δv) Acceleration correction calculated as source-centered velocity minus observer-centered velocity
- Col. 7 (z_c) Corrected redshift velocity calculated as redshift velocity plus negative correction
- Col. 8 (m_B) Stretch luminosity-corrected B-band peak magnitude (from source)

SN	z	θ	$2r \sin (\theta/2)$	$r \sin \theta$	Δ_s	z_c	m_B
(1)	(2)	(3)	(4)	(5)	(6)	(7)	(8)
1996E	0.43	0.6754	0.6627	0.6252	0.037	0.467	22.72
1996H	0.62	0.9739	0.9359	0.8271	0.109	0.729	23.31
1996I	0.57	0.8954	0.8657	0.7804	0.085	-0.655	23.42
1996J	0.30	0.4712	0.4669	0.4540	0.013	0.313	22.28
1996K	0.38	0.5969	0.5881	0.5621	0.026	0.406	22.80
1996U	0.43	0.6754	0.6627	0.6252	0.037	0.467	22.77
1997ce	0.44	0.6912	0.6775	0.6374	0.040	0.480	22.83
1997cj	0.50	0.7854	0.7654	0.7071	0.058	0.558	23.29
1997ck	0.97	1.5237	1.3805	0.9989	0.382	1.352	24.78
1995K	0.48	0.7540	0.7362	0.6845	0.052	0.532	22.92

Table11. Data includes high-redshift and low-redshift supernovae. Source: Riess et al (1998) p. 1020 [76]

SN	z	θ	$2r \sin (\theta/2)$	$r \sin \theta$	Δ_s	z_c	m_B
(1)	(2)	(3)	(4)	(5)	(6)	(7)	(8)
1990O	0.030	0.0471239	0.04721195	0.0471065	0.000013	0.030	16.26
1990af	0.050	0.0785398	0.0785196	0.0784591	0.000061	0.050	17.63
1992P	0.026	0.0408407	0.0408379	0.0408294	0.000009	0.026	16.08
1992ae	0.075	0.1178097	0.1177416	0.1175374	0.000204	0.075	18.43
1992ag	0.026	0.0408407	0.0408379	0.0408294	0.000009	0.026	16.28
1992al	0.014	0.0219911	0.0219907	0.0219894	0.000001	0.014	14.47
1992aq	0.101	0.1586504	0.1584841	0.1579857	0.000498	0.101	19.16
1992bc	0.020	0.0314159	0.0314146	0.0314108	0.000004	0.020	15.18
1992bg	0.036	0.0565487	0.0565411	0.0565185	0.000023	0.036	16.66

1992bh	0.045	0.0706858	0.0706711	0.0706270	0.000044	0.045	17.61
1992bl	0.043	0.0675442	0.06753314	0.0674929	0.000039	0.043	17.19
1992bo	0.018	0.0282743	0.0282734	0.0282706	0.000003	0.018	15.61
1992bp	0.079	0.1240929	0.1240133	0.1237747	0.000239	0.079	18.27
1992br	0.088	0.1382301	0.1381201	0.1377903	0.000330	0.088	19.28
1992bs	0.063	0.0989602	0.0989198	0.0987987	0.000121	0.063	18.24
1993B	0.071	0.1115265	0.1114687	0.1112955	0.000173	0.071	18.33
1993O	0.052	0.0816814	0.0816587	0.0815906	0.000068	0.052	17.54
1993ag	17.69	0.0785398	0.0785196	0.0784591	0.000061	0.050	0.050

Table 12: Data includes only low-redshift supernovae. Source: Perlmutter et al (1999) Calan /Tololo SNe Ia. [77]

N	z	θ	$2r \sin(\theta/2)$	$r \sin \theta$	Δs	z_c	m_B
(1)	(2)	(3)	(4)	(5)	(6)	(7)	(8)
1992bi	0.458	0.7194	0.7040	0.6590	.045	0.503	23.11
1994F	0.354	0.5561	0.5489	0.5278	.021	0.375	22.38
1994G	0.425	0.6676	0.6553	0.6191	.036	0.461	22.13
1994H	0.374	0.5875	0.5791	0.5543	.025	0.399	21.72
1994al	0.420	0.6597	0.6478	0.6129	.035	0.455	22.55
1994am	0.372	0.5843	0.5761	0.5516	.024	0.396	22.26
1994an	0.378	0.5938	0.5851	0.5595	.026	0.404	22.58
1995aq	0.453	0.7116	0.6967	0.6530	.044	0.497	23.17
1995ar	0.465	0.7304	0.7143	0.6672	.047	0.512	23.33
1995as	0.498	0.7823	0.7625	0.7049	.058	0.556	23.71
1995at	0.655	1.0289	0.9841	0.8567	0.127	0.782	23.27
1995aw	0.400	0.6283	0.6180	0.5878	0.030	0.430	22.36
1995ax	0.615	0.9660	0.9289	0.8226	0.106	0.721	23.19
1995ay	0.480	0.7540	0.7362	0.6845	0.052	0.532	22.96
1995az	0.450	0.7069	0.6922	0.6494	0.043	0.493	22.51
1995ba	0.388	0.6095	0.6001	0.5724	0.028	0.416	22.65
1996cf	0.570	0.8954	0.8657	0.7804	0.085	0.655	23.27
1996cg	0.490	0.7697	0.7508	0.6959	0.055	0.545	23.10
1996ci	0.495	0.7775	0.7581	0.7015	0.057	0.552	22.83
1996ck	0.656	1.0304	0.9855	0.8575	0.128	0.784	23.57
1996cl	0.828	1.3006	1.2109	0.9637	0.247	1.075	24.65
1996cm	0.450	0.7069	0.6922	0.6494	0.043	0.493	23.17
1996cn	0.430	0.6754	0.6627	0.6252	0.037	0.467	23.13
1997F	0.580	0.9111	0.8799	0.7902	0.090	0.670	23.46
1997G	0.763	1.1985	1.1281	0.9315	0.197	0.960	24.47
1997H	0.526	0.8262	0.8029	0.7354	0.068	0.594	23.15
1997I	0.172	0.2702	0.2694	0.2669	0.002	0.174	20.17
1997J	0.619	0.9723	0.9345	0.8262	0.108	0.727	23.80
1997K	0.592	0.9299	0.8968	0.8016	0.095	0.687	24.42
1997L	0.550	0.8639	0.8373	0.7604	0.077	0.627	23.51
1997N	0.180	0.2827	0.2818	0.2790	0.003	0.183	20.43

1997O	0.374	0.5875	0.5791	0.5543	0.025	0.399	23.52
1997P	0.472	0.7414	0.7246	0.6753	0.049	0.521	23.11
1997Q	0.430	0.6754	0.6627	0.6252	0.037	0.467	22.57
1997R	0.657	1.0320	0.9868	0.8583	0.128	0.785	22.83
1997S	0.612	0.9613	0.9247	0.8200	0.105	0.717	23.69
1997ac	0.320	0.5027	0.4974	0.4818	0.016	0.336	21.86
1997af	0.579	0.9095	0.8785	0.7892	0.089	0.668	23.48
1997ai	0.450	0.7069	0.6922	0.6494	0.043	0.493	22.83
1997aj	0.581	0.9126	0.8813	0.7911	0.090	0.671	23.09
1997am	0.416	0.6535	0.6419	0.6079	0.034	0.450	22.57
1997ap	0.830	1.3038	1.2134	0.9646	0.249	1.079	24.32

Table 13: The data includes high-redshift and low-redshift supernovae. Source: Perlmutter et al (1999) SCP Data. P. 570 [78]

SN(1)	m_B (2)	z (3)	θ (4)	$r \sin \theta$ (5)	$2r \sin (\theta/2)$ (6)	Δs (7)	z_c (8)
1997ff	27.00	1.7	2.6704	0.4540	1.9447	-1.491	3.191

Table 14: The data includes only the high-redshift supernovae 1997ff. Source: Riess et al (2001) [79]

SN	z	θ	$2r \sin (\theta/2)$	$r \sin \theta$	Δs	z_c	m_B (8)
(1)	(2)	(3)	(4)	(5)	(6)	(7)	
2002fw	1.3	2.0420352	1.7052803	0.8910065	-0.814274	2.114	
2002fx	1.4	2.1991149	1.7820130	0.8090170	-0.972996	2.373	
2002hp	1.305	2.0498892	1.7093709	0.8874134	-0.821957	2.127	
	1.305	2.0498892	1.7093709	0.8874134	-0.821957	2.127	
2002hr	0.526	0.8262389	0.8029366	0.7353879	-0.067549	0.594	
2002kc	0.216	0.3392920	0.3376669	0.3328195	-0.004847	0.221	
2002kd	0.735	1.1545353	1.0914728	0.9146072	-0.176866	0.912	
2003ki	1.41	2.2148228	1.7890893	0.7996847	-0.989405	2.399	
2003kj	1.307	2.0530308	1.7109997	0.8859609	-0.825039	2.132	
2003ak	1.551	2.4363051	1.8769258	0.6482528	-1.228673	2.780	
2003az	1.27	1.9949113	1.6801871	0.9114033	-0.768784	2.039	
2003bd	0.67	1.0524335	1.0045311	0.8686315	-0.135900	0.806	
2003be	0.64	1.0053096	0.9635073	0.8443279	-0.119179	0.759	
2003dy	1.34	2.1048671	1.7372630	0.8607420	-0.876521	2.217	
2003XX	0.935	1.4686946	1.3402056	0.9947921	-0.345413	1.280	
2003cb	0.899	1.4121459	1.2977013	0.9874414	-0.310260	1.209	
2003eq	0.839	1.3178981	1.2245726	0.9681913	-0.256381	1.095	
2003es	0.954	1.4985397	1.3622087	0.9973906	-0.364818	1.319	

Table 15. The data includes 16 Type 1a SNe Ia. Source: Riess et al (2004). Data is incomplete because the authors of this paper were unable to find the effective m_B or distance moduli (column 8) for the supernovae in the Riess et al (2004) paper. Therefore the data is not included in the graphs. However, the corrected redshift values in column (7) are available for comparison with supernovae data. [80]

6. Graphs

i. Linear graph- Perlmutter et al (1999)

Figure 17 shows the linear graph of the data developed by Perlmutter et al (1999) to illustrate the differences between distance using different FRW metrics and intrinsic SNe 1a distance. [81]

The graph shows the redshift data plotted against the effective magnitude of the type 1a supernovae (stretch luminosity-corrected B-band peak magnitude). As can be seen, the relationship is non-linear. The data contains what are referred to as high and low redshift groups of supernovae. Note that the difference between the redshift distance and the supernovae intrinsic distance is resolved by selecting *ad hoc* constants in the FRW equation, which changes the curve shape. [82]

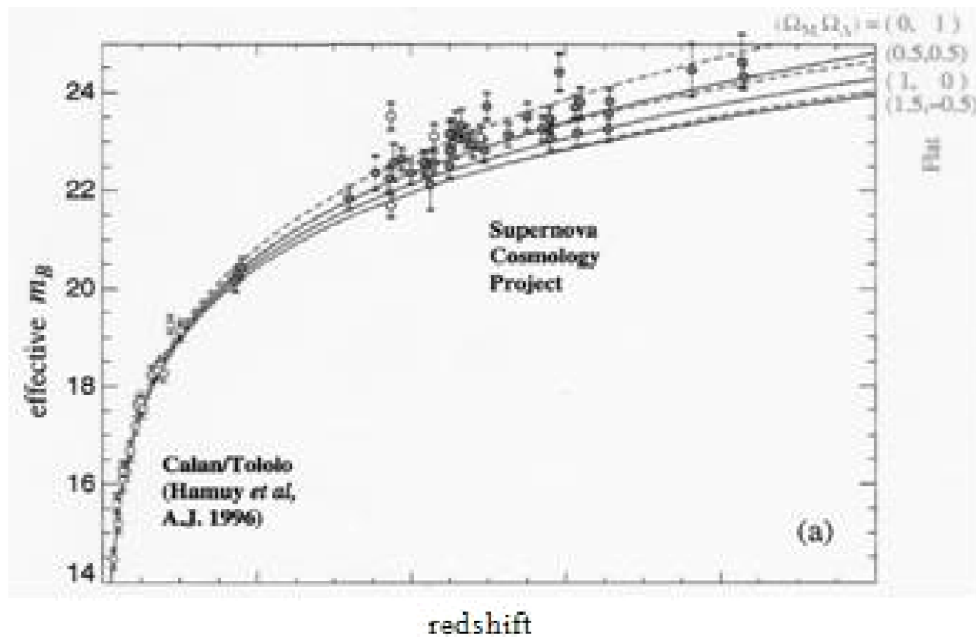


FIG 17: Perlmutter et al (1999) linear graph of supernovae showing the redshift distance shortfall as compared to supernovae intrinsic data. The shortfall is only observable in the high redshift supernovae. It is explained as due to an acceleration of the cosmic expansion which was not predicted in the FRW metric.

ii. New linear graph

The graph in FIG. 18 displays the same data as the top section of the Perlmutter et al (1998) graph shown in FIG. 17, plus data from Riess et al (1998) and one point 1997ff from Riess et al (2001) which has the highest known redshift of any supernova. [83]

The data is being shown in this format to allow the reader to make an easy comparison to the corrected redshift data in FIG. 19 and to the calculated data which was seen back in FIG. 16. As a reminder, FIG. 16 contained both the redshift and corrected redshift curves in the same graph; this was feasible because the curves were derived from equations.

The redshift and corrected redshift graphs in FIG. 18 and FIG. 19 respectively represent actual data points whose natural variability would overlap the two curves and prevent distinguishing one from another, thus they are shown separately.

Note that the redshift curve shown here in FIG. 18 with actual data, closely matches the redshift curve seen previously in FIG. 16), which was derived from the equation

$$(z_a = 1/\cos \theta - 1)$$

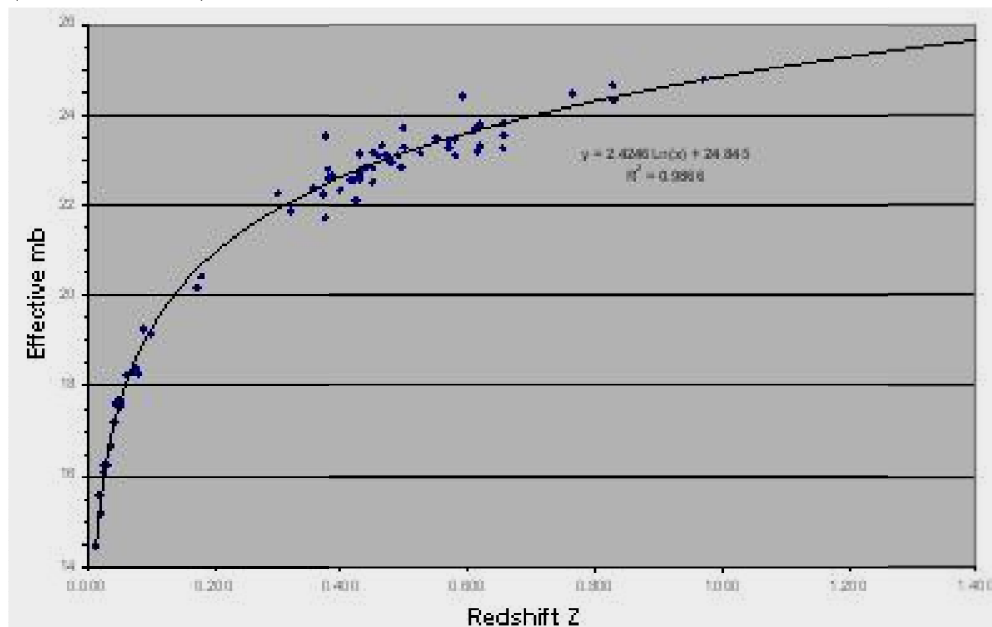


FIG.18. Hubble diagram for Type Ia supernovae from redshift data in Tables 11-15 showing shortfall when compared to supernovae data.

FIG19 shows the effect that $(2r \sin \theta/2 - r \sin \theta)$ had when it was added as a correction to the observed redshift data. As can be seen, the farther away a supernova is, the more the correction adds to the redshift distance.

The correction is accurate within expected limits. The correction caused a 14% increase between the average of the redshift and corrected redshift values for the high z supernovae. . Riess et al (1998) reported that the average increase between the redshift distance and the intrinsic distance was 10% to 15% for the same high z supernovae. [84]

As can be seen, the effect of correction on the redshift distance is the same here in FIG. 19 as it was in Fig. 16 with the calculated function $(1/\cos\theta - 1)$. Since the effect of the correction is the same on observed redshift as it was on the redshift derived from the function, it is reasonable to infer that the observed redshift data is also derived from the same function.

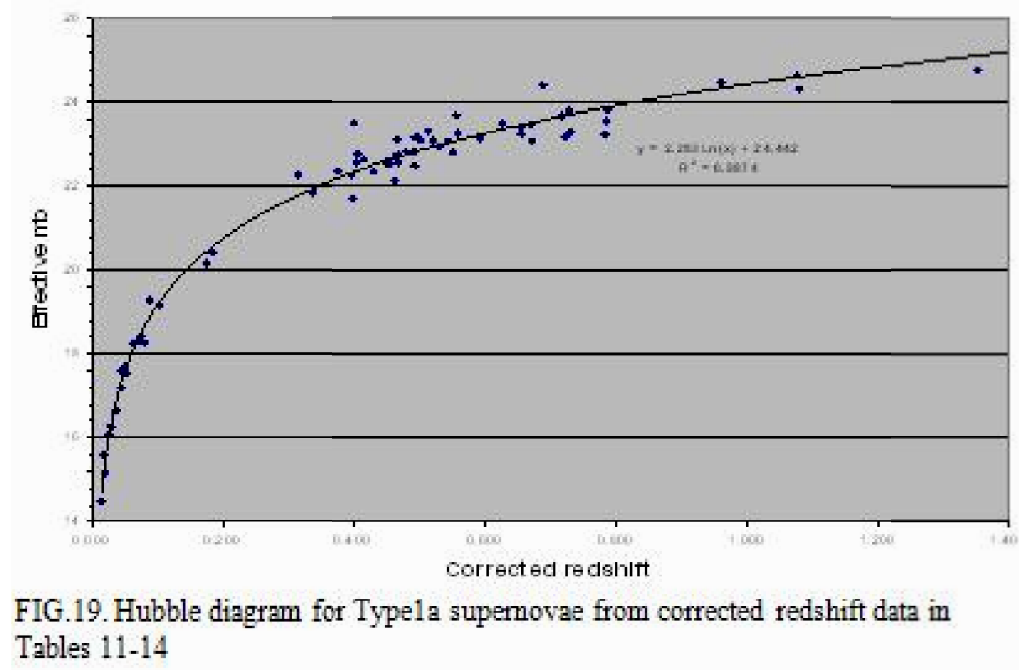


FIG.19. Hubble diagram for Type Ia supernovae from corrected redshift data in Tables 11-14

iii. Logarithmic graph- Perlmutter et al (1999)

FIG. 20 shows the Hubble diagram for 18 low-redshift and 64 high-redshift SNe Ia samples in a logarithmic plot with SNe Ia distances. [85] The logarithmic graph causes the relationship between the supernovae data and the redshift to be linear, so that the difference between them can be more easily seen.

As can be seen, there is a definite slope difference between the high redshift supernovae compared to the low redshift supernovae. Dark energy can be described as the solution for the problem of this slope difference.

According to the theory put forth by Riess et al (1998) and Riess and Turner (2004), the graph shows a time history of the Big Bang expansion. The change in slope represents the change from a matter-dominated era, where matter slowed the expansion, to an energy-dominated era which accelerates the expansion. The larger the redshift, the older the supernova, so we are currently in an accelerated expansion era. [86]

It can be seen that different values for matter, energy and the cosmological constant are entered into the FRW metric to find a linear fit. Currently in order to make the process

work, the cosmological constant, developed by Einstein, must be included. It has a “reverse gravity effect; the further away a star, the greater the repulsive force. [87]

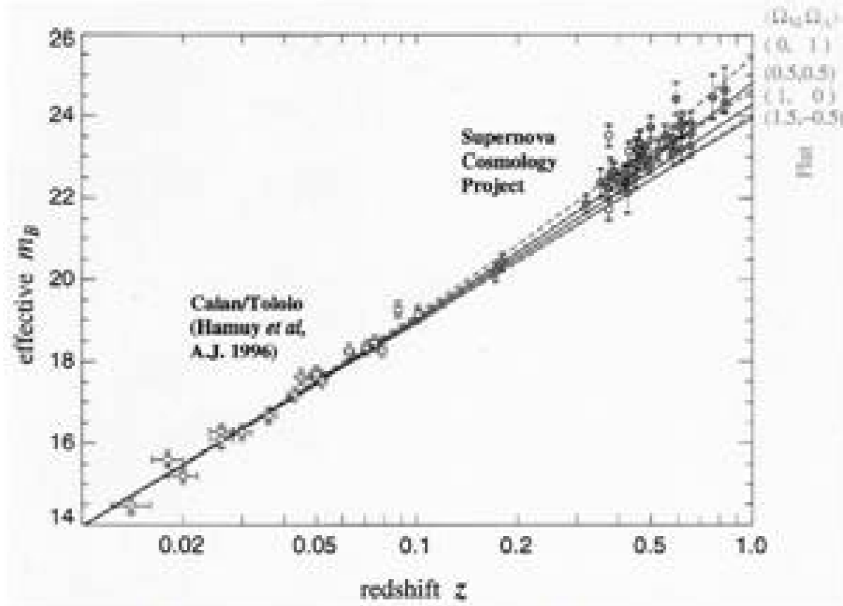


FIG. 20. This figure shows 18 low redshift and 64 high redshift supernovae in a logarithmic graph. Current theory holds that the slope of the high redshift supernovae line is positive due slowing of their expansion in the matter-dominated era.

iv. New log graph

This graph contains the same data as the Perlmutter et al (1999) graph in the top section of FIG. 20 (but also includes 1997ff). The same difference in slope between the high and low supernovae can be seen. However, the explanation for the difference in slope is very different. [88]

The sinusoidal shape of the curve is explained by the equation for the redshift artifact. $1/\cos\theta - 1$. Since redshift is result of observer perspective, not cosmic expansion, the curve represents only distance, not a change in the universe with time. The log function has linearized the curve.

The change in slope of the high redshift supernovae is explained by an untoward effect that occurs when the redshift artifact is used to predict distance. As previously explained, the large perceived parsec causes a shortfall in distance because its large size reduces the unit count for a given distance. the effect is cumulative, so the redshift distance appears to get smaller with distance away from the observer.

When the redshift distance is compared with accurate distance, as seen here with the intrinsic data from the supernovae, the slope of the line increases with distance indicating the short redshift distance, which is on the x -axis. Although only the high redshift supernovae appear to have a positive slope, actually all values of redshift are affected by the shortage.

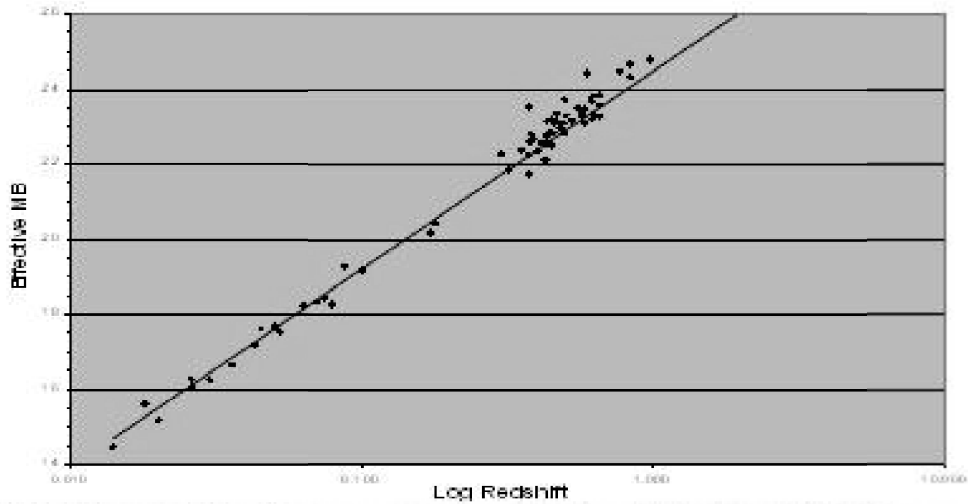
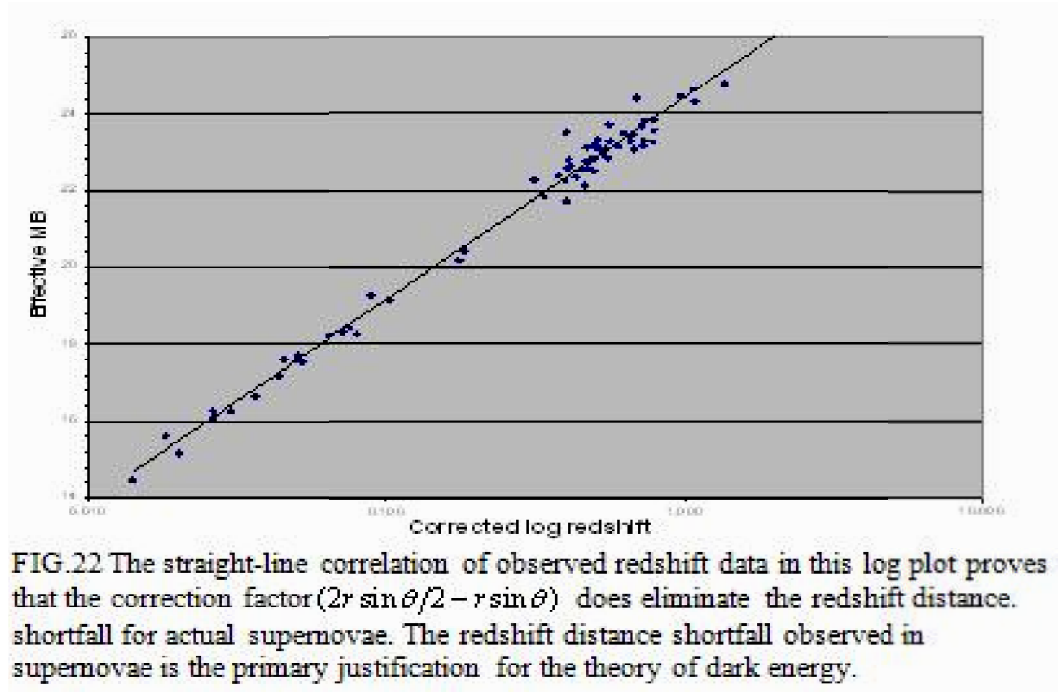


FIG. 21 Log graph of the supernovae data. The shortfall in the redshift-distance relationship accumulates non-linearly so that it becomes larger with distance. Although all the supernovae are affected, only the high redshift show a noticeable change in slope with distance.

As can be seen in the logarithmic graph in FIG.22, the straight-line correlation is proof that the addition of equation $(2r \sin \theta/2 - r \sin \theta)$ values to the real observed redshift values has corrected the distance shortfall. The high and low redshift groups now have the same slope and there is no evidence of any acceleration that requires the explanation of dark energy.



8 Redshift transition point and deceleration

Riess et al (2004) interpreted the sinusoidal redshift artifact function in physical terms as a transition from a constant deceleration caused by dark matter to a constant acceleration caused by dark energy as the universe changed from an era of being matter-dominated to an era of being energy-dominated. [89]

The bottom half of FIG. 22 shows this explanation in a graphical form. The jerk point caused by the transition between the two eras was measured by Riess et al (2004) to be 1.46 ± 0.13 [90]

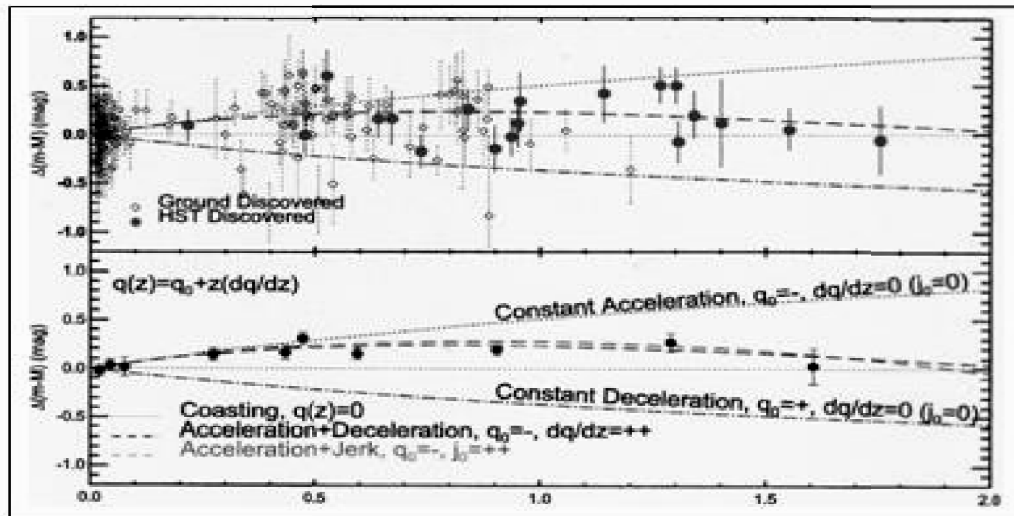


FIG 23 Bottom half of figure shows the redshift transition point at a redshift of 1.46 ± 0.13 set by Riess et al (2004). This change in slope is interpreted in physical terms as the transition from a constant deceleration caused by dark matter to a constant acceleration caused by dark energy.

Since it has been demonstrated that the redshift curve is the result of a function of the redshift artifact, the graph in FIG.23 interprets the curve and straight line interaction geometrically.

In this view, the redshift transition point is explained as the artifact redshift value at which the gap between the sinusoidal error function $(1/\cos\theta - 1)$ and the best fit secant of the lower redshift data first becomes observable.

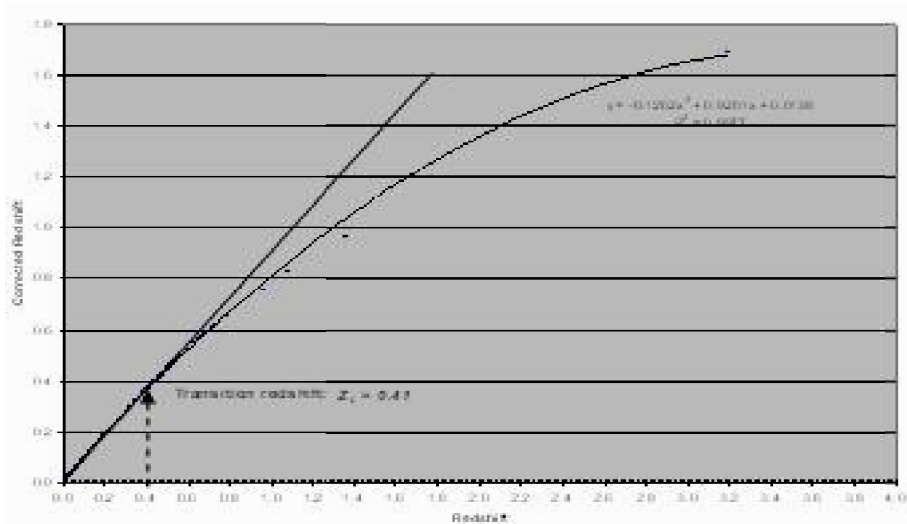


FIG.24.The redshift transition point at 1.41 is explained as where the secant line approximating a linear fit of the lower redshift data separates from the rest of the sinusoidal redshift artifact function. The secant can be difficult to see if the graph is condensed. The redshift value of the separation point 1.46 ± 0.13 was seen as a jerk point in the cosmic expansion by Riess et al (2004).

C. Pioneer anomaly

1. Background

In the early 1970's NASA launched two spacecraft, the Pioneer 10 and 11, into deep space. In order to develop escape velocity from the solar system, the craft used close fly-bys of Jupiter and Saturn as a part of their trajectory. [91] It was discovered while tracking the trajectory of Pioneer 11 that both spacecraft were affected by an unmodeled negative acceleration. The velocity of both the Pioneer 10 and 11 continued to decrease as the spacecraft left the solar system; then became relatively stable. [92]

NASA did not publicize the existence of the error until the early 1990's, believing it was most likely spacecraft-related.¹⁷ In their effort to determine the cause of the anomalous deceleration, NASA, working with JPL, outlined three general areas of possible error in a table that is known as the Error Budget. [93]

The first area is referred to as On-board Generated Systematics. This includes effects such as energy loss and gas leakage. The second area is called Computational Systematics. [94] This area includes other possible causes of the anomaly that are man-made, including mismodeling, calculation drift and periodic terms. The third area is Systematics Generated External to the Spacecraft area. This category includes such environmental forces as solar effects, gravitational attractions and space dust, and also new physics

Most of NASA’s and JPL’s research into the origin of the deceleration has concentrated on the first two areas. As an example, a recent paper from JPL and NASA scientists (Turyshev et al 2011) [95] attributed the anomaly due to the effect of the on-board nuclear heat source.

However, neither the nuclear heat source nor any other function in the On-board Generated Systematics category can explain the time and place of the origin of the anomalous negative acceleration or the mechanism for its increase and decrease during the time spent in the solar system.

2. Correlation with radial velocity

The Pioneer 11 data taken during the spacecraft’s travel in the solar system shows a strong correlation between the anomaly and the radial velocity of the spacecraft. The radial velocity, which in this case is defined as the displacement per time from the tracking stations on Earth, is affected by *both* the spacecraft’s speed and direction.

The spacecraft’s planned interaction with the planets within the solar system caused drastic changes in its direction. The Pioneer 10 and 11 received well recognized scalar speed increases with the “slingshot” effect of their planet encounters followed by slow decreases. Although less well recognized, the spacecrafts’ direction was also changed by these encounters, which modified the ratio of transverse and radial components of their total velocity. Curved motion, which includes a transverse element, for example, lowers the radial component of total velocity significantly.

Radial velocity figures coinciding with anomaly measurements for the spacecraft were not included in the publications reviewed, so values were calculated from the displacement and dates that were supplied. From this data, shown in Table 1, the radial velocity for different distances were calculated. These distances are then matched with the anomaly values in Table 16 from information in Nieto and Anderson (2005). [96]

Displacement AU	Displacement 1.00×10^8 km	X 108 1.00×10^8 km	Date Decimal	Interval years	Interval seconds	Radial Velocity km/s
5.8	8.70	N/A	77.739726603	N/A	N/A	N/A
9.39	1.41	5.39	80.18082192	2.44109589	76982400	7.00
12.16	1.82	4.16	82.52054795	2.339726027	73785600	5.63
14.00	2.10	2.76	83.43561644	0.915068493	28857600	9.56
16.83	2.52	4.25	84.69589041	1.260273973	39744400	10.68
18.90	2.84	3.11	85.567123292	0.871232877	2745200	11.30

Table 16: Calculation of Radial Velocity

The calculated radial velocities for various distances of Pioneer 11’s journey through the solar system can be matched with the published values of the anomaly at those same distances. [97]The advantage of the independent calculation of radial velocity is that there is a time line for the sequence of anomaly values.

The data in Table 17 details the relationship between the radial velocity and the anomaly. There is a very high correlation (0.9) between the anomaly a_p and radial velocity v_{radial} .

Distance	v_{radial}	a_p	σ_p
5.8	*	0.69	1.48
9.38	6.2	**	**
9.39	1.4	1.56	6.85
12.16	10.5	6.28	1.77
14.00	9.6	8.05	2.16
16.83	10.7	8.15	0.75
18.9	11.3	9.03	0.41

Table 17. The correlation coefficient (r^2) between the v_{radial} and a_p values is 0.90.

Two events in the travel of the Pioneer 11 spacecraft in the solar system are especially important in further proving the correlation of radial velocity and the anomaly. The correlation of the anomaly with radial velocity explains both occurrences:

1. The anomaly, even at its lowest level of 1.48, did not appear until 5.8 AU, the distance at which Pioneer 11 intersected Jupiter. [98]

As Figure 24 illustrates, the trajectory of the spacecraft was changed by its meeting with Jupiter. Up to Jovian encounter the Pioneer 11 spacecraft was traveling slowly and maintaining a fairly constant radius about Earth's orbit; producing a very small radial velocity relative to NASA's tracking stations.

After Jupiter, The spacecraft's trajectory straightened, which caused its radial direction to increase significantly and hold steady until intersection with Saturn plus its velocity increased to 48km/s, which at the time was the fastest known relative velocity. The combination increased the spacecraft's radial velocity significantly.

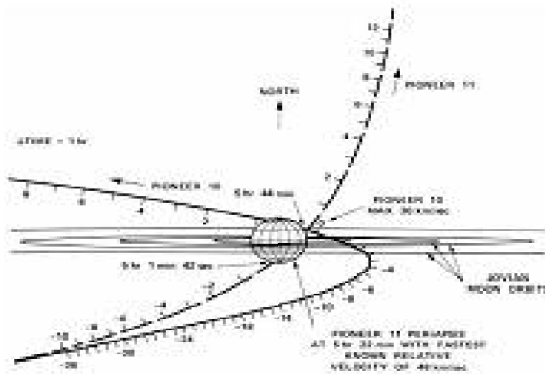


Figure 24: Trajectories of the Pioneer 10 and 11 spacecraft at the Jupiter flyby. Note the increase in radial distance in the two planes of Pioneer 11's trajectory. Its velocity of 48km/s was, at the time, the fastest known.

As can be seen in FIG. 24, the flyby changed Pioneer 11's travel direction away from Earth in two planes. The change increased the radius both along the same plane as measured from the Earth and also almost 90 degrees away from the plane. (Also see FIG. 26 for additional clarity) [99]

Data is not available to quantitate the actual radial velocity at this point as can be seen in Table 12. However, with the demonstrated correlation between radial velocity and the anomaly, the increase in radial direction plus the increase in scalar speed reasonably explains why the anomaly would reach an observable level at the Jovian flyby.

2. The increase in the anomaly between Jupiter and Saturn was recorded as an error.

Figure 25 shows the graph of the early anomaly measurements compared to distance traveled (AU). [100] The second Pioneer 11 point is the result of a data window that included data from both before and after the Saturn encounter. [10]. This paper proposes that what was interpreted as an error was, in fact, actual high reading that were include with low readings in that data window.

It will be shown that the anomaly started at a low value at the Jupiter flyby, then increased to a high value as the radial velocity increased. Then it dropped precipitously as the spacecraft rounded Saturn. The timing of the error at 9.39 AU corresponds to the position where Pioneer's radial velocity goes almost instantly from an average of 6 km/s to less than zero. (See the large view in FIG 24 and the expansion detail in FIG. 26)

Nieto and Anderson in 2005 commented about the error in a foot note: "The second Pioneer 11 data point was stated to have been taken before (or at) Saturn encounter at 9.39 AU. But since Saturn encounter was at 9.38 AU, which would mean there either was a round-off in the distance quoted or the data overlapped the encounter. Either way,

the huge error in this point is anomalous and (sic) therefore it is of great interest to reanalyze this region". [101]

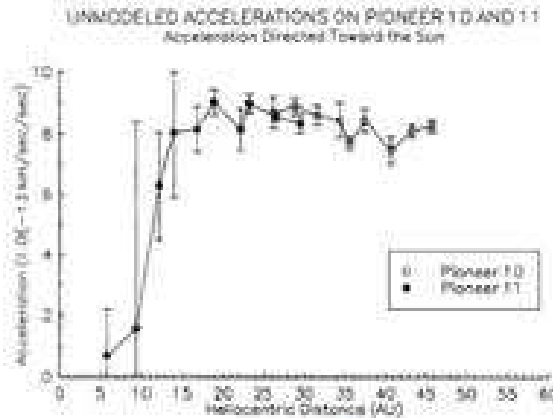


Figure 25: Graph of Early Anomaly Measurements

Note: Large error at second point is actually valid high readings that were unknowingly included in the data acquisition window along with low readings that were also valid.

It was natural for NASA to assume that the anomaly fitted a steady curve and that any high readings found in a data point that was between two low data points would be the result of an error. Upon reanalysis, what was mistakenly called an error was, in reality, valid high readings included in the data point. At a distance of 9.39 AU, which correlates with the Saturn flyby, the anomaly was high, and then fell sharply. The data window included both the high and low readings of the anomaly.

As can be seen in Figure 26, Pioneer 11's path and velocity were changed by the Saturn flyby. It shows clearly that the abrupt change in radial velocity occurred very close to the 9.39 AU point. This corresponds to location of the large recorded error in the second reading. [102]

As can also be seen in FIG.26, after the Jupiter flyby, the Pioneer 11 spacecraft had picked up significant scalar speed and radial direction. This would have caused a large anomaly value for the second data point. However, at Saturn, the spacecraft traveled in a trajectory that roughly paralleled a circular orbit of the sun, with a radius close to Saturn's semi-major axis.

This trajectory caused it to lose most of its radial direction which made the radial velocity drop quickly at the time (9.38 AU) that the second data point was still being collected. Since the data point was collected over a time period, it included both the high and low

velocities. Because the resulting high anomaly value didn't fit the curve, NASA considered it an outlier, which explains the very large error in the second data point.

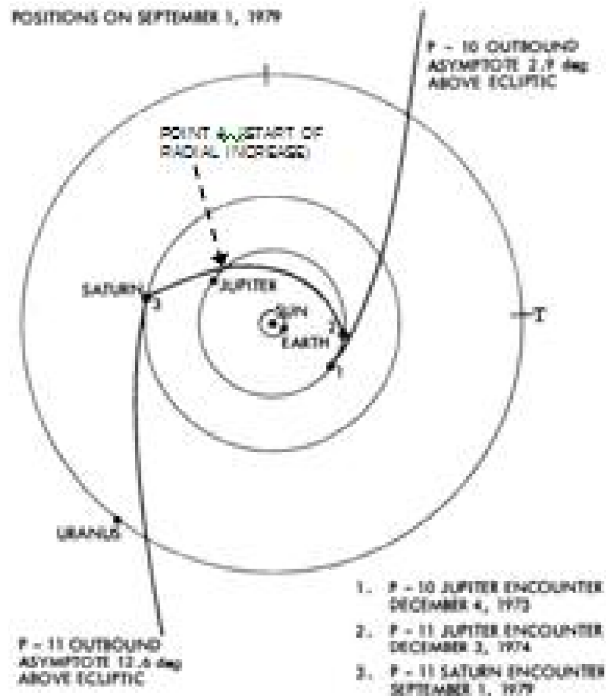


FIG.26. View of the travel of Pioneer 10 and 11 spacecraft in the solar system. Note at Point A, after the Jupiter flyby, that Pioneer 11's radial direction and scalar speed increases. Also note the abrupt direction change during the Saturn encounter, which significantly reduces the spacecraft's radial direction and thus radial velocity relative to Earth.

Figure 27 shows this path in detail. As can be seen, the radial velocity actually went negative at about 300 days as the spacecraft followed this path. [103] Eventually, the spacecraft's speed (solar escape velocity) was too great to maintain the circular trajectory and it pulled away after about 200 days of orbital travel. (at about day 420 in Figure 25). After leaving orbit, the spacecraft's radial velocity increased slowly because of its oblique angle of trajectory relative to Earth.

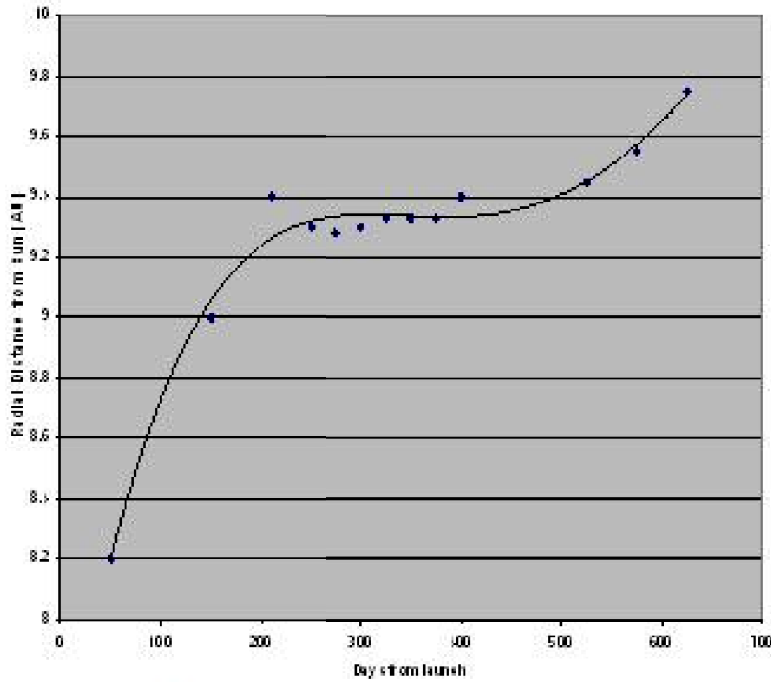


Figure 26: Detail of Pioneer 11 before and after Saturn Flyby
Radial distance from the Sun (in AU) vs. time (in days
starting with 1 Jan. 1979)

In summary, the decay of a nuclear heat source cannot explain the reason for the particular beginning point for the anomaly, nor can it explain the reason for the extreme error in the second data point. As will be seen, the application of the same equation used to predict the Hubble constant and to correct the redshift-distance equation also predicts the Pioneer anomaly almost perfectly.

2. Calculation

The anomaly is based on a comparison with a calculated model. [104] The radar measurement included travel both to and from the spacecraft; hence the error (a_p) as measured by Doppler radar must be divided by a factor of two in the equation:

$$\left[v_{obs}(t) - v_{model}(t) \right]_{DSN} = -v_0 \frac{2a_p t}{c} \quad (52)$$

$$v_{model} = v_0 \left[1 - \frac{2v_{model}(t)}{c} \right] \quad (53)$$

v_{obs} is the frequency of the retransmitted signal received by the tracking station (an active return signal, not a passive “bounce” was sent by the spacecraft when the transmitted

signal was received). ν_{model} is the frequency predicted by NASA based on expected variable values. ν_0 is the reference frequency. DSNE is an acronym for Deep Space Network. [105]

The anomaly causes an increase in the wavelength of the radar signals as the distance from Earth increases. The resulting redshift causes the spacecraft to exhibit negative acceleration when compared to the mathematical model used by NASA.

The same equation that was used to calculate the Hubble constant is used to calculate the Pioneer anomaly. The values differ between the two applications for the velocity, angle and radius. The result for the Hubble constant was based on $\Delta\nu$ per a velocity of 1km/s per a radius of 1Mpc. The result for the Pioneer anomaly is based on the velocity of the spacecraft ν .

$$\Delta\nu = \left[2r \sin\left(\pi/4 \frac{\nu}{2c}\right) \right] - \left[r \sin\left(\pi/4 \frac{\nu}{c}\right) \right]. \quad (54)$$

The velocity ν of an object moving relative to the observer can be determined by the Doppler Effect on the frequency of the radar signal. The following equation multiplies the speed of light by the percent of frequency change [106]

$$\nu = c \frac{(f_{obs} - f_{emit})}{f_{emit}} \quad (55)$$

The calculated speed of light has the $\Delta\nu$

$$\nu = [c + \Delta\nu] \frac{\Delta f}{f_{emit}} \quad (56)$$

The $\Delta\nu$ manifests as a negative acceleration of the moving object.

$$\nu - \Delta\nu = c \frac{\Delta f}{f_{emit}} \quad (57)$$

The error becomes negative.

$$-\Delta\nu = \left[2r \sin\left(\pi/4 \frac{\nu}{2c}\right) \right] - \left[r \sin\left(\pi/4 \frac{\nu}{c}\right) \right]. \quad (58)$$

First, the angle is calculated for the velocity of each spacecraft and the results are shown in the following two tables. [107]

pi/4	v	c	θ
(radians)	(km/s)	(km/s)	radians * (km/s/km/s)
0.785398163	10.45	299792.458	2.737697560E-05

Table 19: Angle θ at a radial velocity of 10.45 km/s for Pioneer 10

pi/4	v	c	θ
(radians)	(km/s)	(km/s)	radians* (km/s/km/s)
0.785398163	11.33	299792.458	2.968240512E-05

Table 20: Angle θ at a radial velocity of 11.33 km / s / s for Pioneer 11

The next step is to use the appropriate calculated angle with a radius of one light second expressed in km, to calculate the Δv per kilometer per second per second by subtracting the Cartesian velocity ($r \sin \theta$) from the polar velocity ($2r \sin \theta/2$):

Avg. Velocity (km/s)	Function	Δv values (km/s/s)
10.45	$2r \sin \theta/2$	8.207410807247
	$r \sin \theta$	8.207410806478
	Difference	0.000000000769

Table 21: Calculation of Δv for Pioneer 10 spacecraft is $-7.69 \times 10^{-10} \text{ km / s / s}$.

Velocity (km/s)	Function	Δv values (km/s/s)
11.33	$2r \sin \theta/2$	8.898561119066
	$r \sin \theta$	8.898561118986
	Difference	0.000000000980

Table 22: Calculation of Δv for Pioneer 11 spacecraft is $-9.80 \times 10^{-10} \text{ km / s / s}$.

The average Δv for both spacecraft is displayed in Table 18.

Spacecraft	Δv values (km/s/s)
Pioneer 10 Δv	0.000000000769
Pioneer 11 Δv	0.000000000980
Average Δv	0.0000000008745

Table 23: The average Δv for both Pioneer 10 and 11 is $-8.745 \times 10^{-10} \text{ km / s / s}$

As covered in the section on the effect of Δv on radar, the Δv makes it appear that an object moving away from the observer has a small blue shift on top of the expected red shift. This blue shift manifests as a negative acceleration.

$$v - \Delta v = c \frac{\Delta f}{f_{emit}} \quad (59)$$

$\Delta v = 8.745 \times 10^{-10} \text{ km/s/s}$ which manifests as negative acceleration of Pioneer spacecraft

NASA's value for the Pioneer anomaly is $-8.74 \times 10^{-10} \text{ km/s/s}$. (Anderson et al 1995). The error accelerated the speed of the radar light signal used to measure the radial velocity of the Pioneer spacecraft. The increase in light speed is seen as a negative acceleration in the velocity of the spacecraft [108]

NASA developed an error budget by totaling all of the possible sources of experimental error. The total allowance for error as determined by this budget is $\pm 1.33 \times 10^{-10}$, which equals $\pm 15\%$ of the average value. The predictions are all well within this limit. [109]

VII. DISCUSSION

A. Proofs of the theory

Proofs of this theory include both direct and indirect forms. For direct proof, the basic concept, which was derived from first principles, accomplished the following:

1. Derived the Hubble Constant
2. Developed the curves for recession velocity, redshift and the scale factor
3. Corrected the redshift distance shortfall that was the *raison d'être* for dark energy
4. Predicted the Pioneer anomaly.

Each of these applications was demonstrated to be within experimental limits when tested on data.

The construction of a complex *ad hoc* equation to fit a single set of data may be explained by curve fitting; however, deriving a simple equation that very precisely fits several different data sets is unlikely to be a coincidence. Further, the logic and mathematics of the fit is clear and straightforward, with no requirement for unseen or dark forces.

As indirect proof, the theory was shown to be in agreement with several predictions of the special and general theories of relativity

1. The theory predicts the presence of a radial component in transverse distance, which was confirmed by the Transverse Doppler Effect (TDE).
2. The theory predicts that the redshift equation is $1 + z = 1/\cos\theta$; which was confirmed by the special theory of relativity equation $1 + z = 1/\sqrt{1 - v^2/c^2}$, when it was demonstrated that $\cos\theta = \sqrt{1 - v^2/c^2}$.
3. The theory qualitatively predicts the sinusoidal shape of the FRW curves for redshift, v/c , and the scale factor, which are confirmed by comparing to observation.
4. The theory derives the space-time interval and the relationship between coordinate time and proper time from the difference between Euclidean and taxicab geometries.

Finally, the fact that the theory almost exactly matches most nominal values in the applications is doubly reassuring. When the value derived from first principles is so closely confirmed by experimental results, it means that both methods are very reliable.

B. Implications of the theory

1. The use of the observer-centric perspective, with Cartesian coordinates and 1-norm Minkowski distance, causes an error in the Pythagorean Theorem when measuring distance or velocity in reference to a point source of energy or force.

This is because the Pythagorean equation $dl^2 = x^2 + (cdt)^2$ was derived in taxicab geometry and therefore doesn't follow the spectroscopic definitions of radial and transverse directions. This equation assumes that it is l that has the radial component; because distance l begins and ends with a different y coordinate value. However, spectroscopically, it is x that has the radial component because it begins and ends with a different r coordinate.

The spectroscopic definition of distance in Euclidean geometry requires a different form of the Pythagorean equation so that $dl^2 = x^2 - (cdt)^2$. This form shows it is x that has the radial component. However, it only provides valid distances when t is negative so that $dl^2 = x^2 - (-cdt)^2$ which returns to $dl^2 = x^2 + (cdt)^2$.

This has implications to Euler's formula which states that, for any real number x , $e^{ix} = \cos x + i \sin x$, where e is the base of the natural logarithm, i is the imaginary unit, with the argument x given in radians. Since the trigonometric functions are derived from the Pythagorean Theorem, Euler's formula is in taxicab geometry. It could be translated into Euclidean geometry for better understanding.

2. There are strong indications in this paper that the function of the special theory of relativity is to convert distance from taxicab to Euclidean geometry. When time is defined by light traveling from a point source, the 1-norm function, which measures time

with the y coordinate, fits the definition of coordinate time and the 2-norm function, which measures time with the r coordinate, fits the definition of proper time.

In terms of four-dimensional spacetime, proper time is defined as the arc length s between two events E_1 and E_2 in three-dimensional (Euclidean) space. By contrast, coordinate time Δt is the time between E_1 and E_2 events as measured by an observer at E_1 in his or her frame of reference.

The function $1/\cos\theta$ was shown to equal the relativistic gamma $\gamma = 1/\sqrt{1-v^2/c^2}$. Serious treatment of this subject is far beyond the scope of this paper, but a paper that explains the predictions of the special theory of relativity in geometric rather than physical terms is planned.

3. With redshift demonstrated to be the result of a perspective artifact, the main evidence for cosmic expansion has been lost. Cosmic expansion is, in turn, the main evidence for the Big Bang theory. Although there is other evidence supporting it, the Big Bang theory does not appear viable without cosmic expansion.

Similarly, with the shape of the derived scale factor curve showing an inflation-like increase, inflation the result of a physical phenomenon or is it a product of geometry?

4. With the difference in luminosity distances explained by an artifact caused by the difference in perspectives, the need for the existence of dark energy would seem to have been eliminated.

VIII. CONCLUSIONS

1. The recession velocity discovered by Edwin Hubble is an artifact of observation caused by the measurement of light emitted from a point source using the observer-centered perspective with taxicab geometry.
2. Redshift is the observable result of the velocity artifact.
3. The FRW curves can be explained by the sinusoidal functions derived from the difference in perspectives, rather than a record of the physical expansion of the cosmos shaped by matter, energy and the cosmological constant
4. The shortfall of the luminosity distance calculated using the FRW redshift-distance method compared to SNe type1a intrinsic luminosity distance is the result of the Earth observer's use of a longer perceived parsec unit. A longer unit makes the number of units per distance less and the error accumulates with distance. the shortfall is corrected by the addition of the perspective difference in distance.

5. The Pythagorean Theorem is not applicable when measuring light from a point source.

6. The Pioneer anomaly is the result of the longer parsec unit (which converts to a longer kilometer). The longer unit makes the number of units per distance less and the error accumulates with distance. As the distance appears to shorten, the spacecraft appears to decelerate.

IX. ACKNOWLEDGEMENTS

We thank Bryan Webber for his longsuffering endurance of hours of listening to the latest progress on “The Project” and for the helpful critique he offered.

X. FOOTNOTES

1. Rabin, Sheila, "Nicolaus Copernicus", *The Stanford Encyclopedia of Philosophy (Fall 2010 Edition)*, Edward N. Zalta (ed.), <http://plato.stanford.edu/archives/fall2010/entries/copernicus/>.

2. The source-centered distance d_h between objects at any instant is defined as the difference between their polar radial and angular magnitudes as measured from the light source's origin which is unchanging relative to the objects.

3. For a real number $p \geq 1$, the p -norm or L^p -norm of a distance x is defined by.

$\|x^p\| = \left(|x_1^p| + |x_2^p| + \dots + |x_n^p| \right)^{1/p}$. The 2-norm corresponds to Euclidean distance. (The 1-norm is the norm that corresponds to the Manhattan distance). With a simple path, the distance traveled by the object is the square root of the sum of the x-component distance squared and the y-component distance squared. The vector norm is Euclidean or L^2 norm

$$(p, q) = \sqrt{\sum_{i=1}^n (p_i - q_i)^2} .$$

mathworld.wolfram.com/Distance.html

4. An incremental change in radius caused by an incremental change in circumference is not affected by the magnitude of either the radius r or the circumference C .
www.newton.dep.anl.gov/askasci/math99/math99160.htm

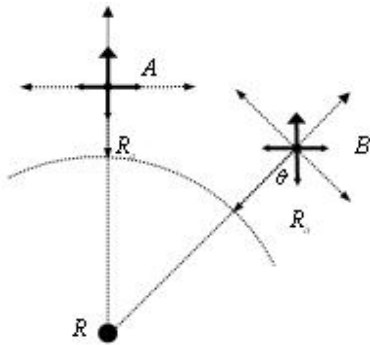
5. Lecture 4 -- Geocentric and Heliocentric Systems
www2.astro.psu.edu/users/rbc/a1/lec4n.html

6. The observer-centered distance d_g is the difference between an object's Cartesian radial y and transverse x magnitudes as measured from the observer's origin.

Definition of observer-centered

www.merriam-webster.com/dictionary/observer-centered -

7. As can be seen, when A, as the observer, sees B in the same x-y coordinate system (heavy lines), then B's relationship with R is then not the same as A's. If A and B have independent relationships (light lines) with R, then they both have the same relationship with R.



8. The norm in this case is rectilinear (taxicab) or L_1 norm: $d_1(p, q) = \sum_{i=1}^n |p_i - q_i|$. In the observer-centered perspective, the radial distance ($r = \sqrt{y^2 + x^2}$) is still a possible path, but it has no definition in terms of radial or transverse. In this geometry, radial distance is defined as y and the transverse distance is defined as x . The total path from the star to the 1-norm Earth position is the L-shaped path formed by the addition of the y and the x coordinate distances ($x + y$)

Eugene F. Krause (1987). *Taxicab Geometry*, Dover. ISBN 0-486-25202-7

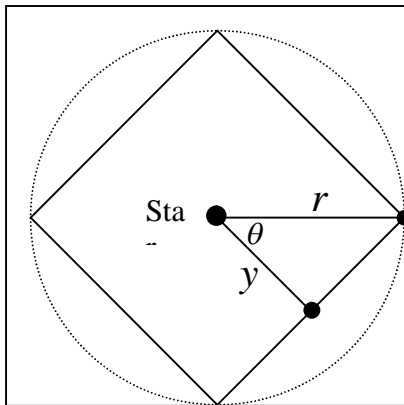
9. A circle is defined as a set of points with a fixed radial distance r from a center point. In taxicab geometry, circles are squares with sides oriented at a 45° angle to the coordinate axes. In the Euclidean metric, each side of the square would have length $\sqrt{2}r$, while in taxicab geometry, its length is $2r$. Thus, a taxicab circle's circumference is $8r$, which makes 4 the value of a geometric analog to π in this geometry
jwilson.coe.edu/MATH7200/Taxicab/TaxiCab.html

10. The following figure shows a comparison of the Euclidean and taxicab wave fronts of a star. The radius of the Euclidean circle is r and the radius of the taxicab circle is y . The diamond-shaped line is the taxicab circumference which compares with the Euclidean circumference which is the normally expected circular shape.

The circumference of the taxicab circle in the figure is $C = 2 + 2 + 2 + 2 = 8$. The definition of π is the ratio of the circumference of a circle to twice its radius. As can be seen in the figure, that definition gives the value of π in taxicab geometry of

$$\pi_t = 8/2 * 1 = 4.$$

The formula for the circumference of a taxicab circle is $c = 8r$ or using the taxicab π_t value, it becomes $C = 2\pi_t r$ which has the same form as the Euclidean formula for a Euclidean circle:



taxicabgeometry.net/geometry/circles

11. Euler, Russell and Jawad Sadek. *The π s Go Full Circle*, Mathematics Magazine, Vol. 72, No. 1 (Feb 1999), pp. 59-63.

12. As will be seen in FIG. 2, the radius r , which is a polar coordinate, can be represented by $\sqrt{y^2 + x^2}$ in the Cartesian system, when x is infinitesimal. In this case, as x approaches 0, then $\sqrt{y^2} = y$. This makes $y = r$ so that both represent the polar radial distance. The sum of the infinitesimal x rectilinear distances approximates a curved polar arc $r\theta$, so that the transverse distances are also equal.

13. The radial direction is defined as that direction relative to a light source in which travel causes the observer to perceive a change in wavelength. The transverse direction is defined as that direction relative to a light source in which travel does not cause the observer to perceive a change in wavelength. Note that a tangential direction does not maintain a constant radial distance from the light source and therefore movement in this direction has both a transverse and a radial component and will cause the perception of a change in wavelength.

14. All distances measured by radar are rectilinear. Thus, the formula that matches the distance of one AU is the chord $2r \sin \theta/2$, not the arc $r\theta$. Since, the arc and the chord begin and end at the same radial distance, there is no net radial change with either distance.

15. www.newton.dep.anl.gov/askasci/math99/math99160.htm

16. cims.nyu.edu/~kiry1/Calculus/Section_7.4--Arc.../Arc_Length.pdf

17. The radius r , which is a polar coordinate, can be represented by $\sqrt{y^2 + x^2}$ in the Cartesian system, when x is infinitesimal. In this case, as x approaches 0, then $\sqrt{y^2} = y$. This makes $y = r$ so that both represent the polar radial distance. The sum of the infinitesimal x rectilinear distances approximates a curved polar arc $r\theta$, so that the transverse distances are also equal.

18. The original radial distance y_2 from FIG.2 is measured in Euclidean geometry equals r . The new radial distance y_2 , measured in taxicab geometry, equals $r/\cos\theta$.

19. When the Sun and Earth are on the same plane as the star, the alignment can be changed simply by taking the measurements at a different point in Earth's orbit around the Sun. For the same radial distance r to the star, the Earth will be in the quadrant of the orbit nearest the star; for the same radial distance y to the star, the Earth will be on a line with the Sun that is orthogonal to the line from the star. When the Sun and the Earth are not on the same plane as the star, the alignment must be virtual, that is, a mathematical adjustment in distance must be made in order to change the alignment.

20. In terms of Euclidean geometry, the Cartesian x distance begins and ends with a different radial distance (r) from the star. In terms of the taxicab geometry, the x distance begins and ends with the same radial distance (y) from the star. The opposite is true for the l distance. In Euclidean geometry, it begins and ends with the same radial distance (r) from the star, but in taxicab geometry, it begins and ends with a different radial distance (y) from the star.

21. The spectroscopic test determines whether a direction has a radial component by moving in that direction and checking for a change in wavelength. If a change in wavelength occurs, then the radial distance from the light source must have changed during movement and therefore, there is a radial component. If the wavelength does not change, then there is no radial component and the direction is all transverse. As mentioned previously, the only all transverse distance is an arc segment of the wavefront circumference of the light source.

22. When the radial distance is defined as cdt , because c is a constant, the variable in the radial distance interval is the time interval dt^2 . Because the transverse distance dl has no radial distance, it has no time component. However, the interval dx has both a radial and a transverse component, so it fits the definition of the space-time interval ($dx^2 = dl^2 - (cdt)^2$). However, there is a complication. In order for the Pythagorean Theorem to match the spectroscopic definitions of radial and transverse distances, the time component dt^2 must be a component of x , not of l . Therefore, the spectroscopically-correct equation is

$$dx^2 = dl^2 + (cdt)^2 .$$

As can be seen, this equation is still not valid since the dl distance is actually larger than the x distance, not smaller as shown in the equation. In order for this equation to fit the observed distance magnitudes, the function dt^2 must be negative. $dx^2 = dl^2 + (c(-dt))^2$.

In this form, the equation fits the spectroscopic definitions of radial and transverse direction and agrees with the observed distance magnitudes. $dx^2 = -(cdt)^2 + dl^2$.

However, because cdt^2 is negative, the square root of the function is imaginary.

23. www.merriam-webster.com/dictionary/parallax

24. It might seem that the parsec unit should have been defined in Euclidean geometry using the equation $pc(r) = x/\sin \theta$.

However, if this equation were used to define the parsec, the magnitude of radial distance would change between the Sun and the Earth, even though they are on the same x baseline, which makes no sense in taxicab geometry. In addition, this equation would leave the Cartesian y axis magnitude largely undefined in terms of radial distance since the y axis only equals r when $x = 0$.

scienceworld.wolfram.com/astronomy/Parsec.html

25. With the angle $p = \theta$, and the wavefront travel distance r to the Earth as ct , then the wavefront travel distance y to the Sun can be expressed as $ct \cos \theta$. Thus, by dividing by both distances by c , the relationship of proper time to coordinate time is a factor of $ct/c = ct \cos \theta/c$.

The relationship between r and y can be expressed in terms of the x distance, using the Pythagorean Theorem $((ct)^2 = (ct \cos \theta)^2 + x^2$.

The equation is first normalized to the Earth's frame of reference by dividing through both sides of the equation with $(ct)^2$, which creates dimensionless units whose magnitude is made relative to ct .

$$\frac{(ct \cos \theta)^2}{(ct)^2} = \frac{(ct)^2}{(ct)^2} - \frac{x^2}{(ct)^2}$$

The equal function is canceled to make unity.

$$\frac{(ct \cos \theta)^2}{(ct)^2} = 1 - \frac{x^2}{(ct)^2}$$

Taking the square root of both sides and simplifying provides the ratio of the wavefront distances from the two frames of reference.

$$\frac{c \cos \theta t}{ct} = \sqrt{1 - \frac{x^2}{(ct)^2}}$$

The common term ct on the left side can be canceled,

$$\cos \theta = \sqrt{1 - \frac{x^2}{(ct)^2}}$$

. Next, the position x^2 is expressed as velocity times time $(vt)^2$

$$\cos \theta = \sqrt{1 - \frac{(vt)^2}{(ct)^2}}$$

Dividing by t gives the ratio in terms of velocity

$$\cos \theta = \sqrt{1 - \frac{v^2}{c^2}}$$

Since proper time is t and coordinated time is $t \cos \theta$, the conversion factor is $1/\cos \theta$ which, as can be seen, is equal to the relativistic gamma $\gamma = 1/\sqrt{1 - v^2/c^2}$

26. www.merriam-webster.com/dictionary/proper

27. Artifact definition: any perceived distortion or other data error caused by the instrument of observation.

www.websters-online-dictionary.org/definition/artifact

28. The current scientific method does contain a procedure for excluding data with systematic errors; for instance, it does not require the observer's frame of reference be aligned with the force or energy source. It only deals with excluding observations with random errors, since it requires reproducibility

29. The calculation of Hubble's constant is shown in Equation 11.

30. Hubble, Edwin, "A Relation between Distance and Radial Velocity among Extra-Galactic Nebulae" (1929) *Proceedings of the National Academy of Sciences of the United States of America*, Volume 15, March 15, 1929: Issue 3, pp. 168–173, communicated January 17, 1929

31. The cumulative effect of a small error per unit was exemplified in 1999 with the crash of the Mars Climate Orbiter. The cause was traced to an unrecognized substitution between metric and English force units. The difference in force between a single English pound of force unit ($lb_f = lb_m \cdot g_n$) and a single metric Newton unit ($N = kg \cdot m / s^2$) is too small to have a significant effect on the path of the space craft, however, the accumulation of the error from many units caused the Orbiter computer to direct the space craft to enter the Mars atmosphere at too low an altitude causing the craft's disintegration.

en.wikipedia.org/wiki/Mars_Climate_Orbiter

32. A circle is defined as a set of points with a fixed radial distance r from a center point. In taxicab geometry, circles are squares with sides oriented at a 45° angle to the coordinate axes. In the Euclidean metric, each side of the square would have length $\sqrt{2}r$, while in taxicab geometry, its length is $2r$. Thus, a circle's circumference is $8r$, which makes 4 the value of a geometric analog to π in this geometry
jwilson.coe.edu/MATH7200/TaxiCab/TaxiCab.html

33. en.wikipedia.org/wiki/Skinny_triangle

34. www.newton.dep.anl.gov/askasci/math99/math99160.htm

35. Hubble, Edwin, "A Relation between Distance and Radial Velocity among Extra-Galactic Nebulae" (1929) *Proceedings of the National Academy of Sciences of the United States of America*, Volume 15, March 15, 1929: Issue 3, pp. 168–173, communicated January 17, 1929

36. It is well understood that Galilean relativity works well at low speeds. The velocities used in this paper are less than 12km/s and thus are non-relativistic.
physics.ucr.edu/~wudka/Physics7/Notes_www/node47.html

37. scienceworld.wolfram.com/astronomy/Parsec

38. www.astro.cornell.edu/academics/courses/astro201/hubbles_law

39. scienceworld.wolfram.com/astronomy/Parsec

40. The distance modulus is calibrated in units of megaparsecs based on the relationship between the flux of two different stars with their apparent magnitudes

F_1, F_2 are the individual flux from each star one and m_1, m_2 are their individual apparent magnitudes

$$\frac{F_1}{F_2} = 100^{(m_2 - m_1/5)}$$

However, for astronomy use, this ratio between two stars is modified to work with one star at two different distances. In this modification, F is the flux of the star at a given distance and F_{10} is the flux of the same star at 10 parsecs further away and the difference in magnitude is the difference between the absolute magnitude and the apparent magnitude of the one star.

$$\frac{F_{10}}{F} = 100^{(m - M/5)}$$

This equation is calibrated in distance r (in parsecs) by the relationship between flux F and luminosity L :

$$F = \frac{L}{4\pi r^2}$$

When this function is substituted for flux in the ratio, luminosity is canceled (luminosity is an intrinsic property of the star and does not depend on distance).

$$\left(\frac{r}{10}\right)^2 = 100^{(m - M)/5}$$

Rearranged, this is seen as the distance modulus

$$m - M = 5 \log_{10} \left(\frac{r}{10}\right)$$

astronomy.swin.edu.au/cosmos/D/Distance+Modulus

41. en.wikipedia.org/wiki/Hubble's_law

42. en.wikipedia.org/wiki/Hubble's_law

43. map.gsfc.nasa.gov/universe/uni_expansion.html

44. ned.ipac.caltech.edu/help/zdef.html

45. Hubble, Edwin, "A Relation between Distance and Radial Velocity among Extra-Galactic Nebulae" (1929) *Proceedings of the National Academy of Sciences of the United States of America*, Volume 15, March 15, 1929: Issue 3, pp. 168–173, communicated January 17, 1929

46. starchild.gsfc.nasa.gov/docs/StarChild/questions/redshift.html

47. Scienceworld.wolfram.com > ... > Relativity Theory > Special Relativity

48. Herbert E. Ives and G. R. Stilwell undertook the task of performing the experiment and they came up with a very clever way of separating the much smaller TDE from the much bigger longitudinal Doppler Effect. The experiment was performed in 1938 and it was repeated multiple times.

Hoffman-Wellenhof, H. Lichtenegger and J. Collins, *GPS Theory and Practice*, 2nd ed. (Wien: Springer, 1993). pp. 82-83 and 106-109

49. Apparent redshift without radial motion was first predicted in by Einstein in 1905. As explained within special relativity, the Lorentz factor is dependent only on the magnitude (speed) of motion and is not affected by its vector direction. The relativistic correction made to the Doppler Effect equation therefore includes effects from both radial and transverse motion.

Albert Einstein, *Relativity, The Special and General Theory*, (Wings Books, New York, 1961) p.87

50. en.wikipedia.org/wiki/Relativistic_Doppler_effect

51. The parallax method is the fundamental calibration step for the distance ladder. Ground-based telescope measurements of parallax angle is limited to about 0.01 arcseconds, and thus to stars no more than 100 pc distant
en.wikipedia.org/wiki/Parsec

52. Astro.unl.edu > NAAP Labs

49. Hubble, Edwin, "A Relation between Distance and Radial Velocity among Extra-Galactic Nebulae" (1929) *Proceedings of the National Academy of Sciences of the United States of America*, Volume 15, March 15, 1929: Issue 3, pp. 168–173, communicated January 17, 1929

53. www.mathopenref.com/similartriangles.html

54. A normalized vector maintains its direction but its length becomes one. The resulting vector is often called a unit vector. A vector is normalized by dividing the vector by its own length..

mathworld.wolfram.com > Algebra > Vector Algebra

55. Unit vectors have a length of one. If you have a particular vector \mathbf{v} you can use it to make a unit vector. This is called normalizing the vector: 1. Calculate the length of \mathbf{v} , $|\mathbf{v}|$. 2. Scale \mathbf{v} by dividing by its length: $\mathbf{v} / |\mathbf{v}|$.
chortle.ccsu.edu/VectorLessons/vch06/vch06_10.html
56. background.uchicago.edu/~whu/courses/Ast321_11/ast321_1.pdf
57. Tamara M. Davis, Charles H. Lineweaver, "Superluminal Recessional Velocities".
 ArXiv: astro-ph/0011070 [astro-ph]. doi:10.1063/1.1363540 (2000)
58. Tamara M. Davis, Charles H. Lineweaver "Superluminal Recessional Velocities".
 ArXiv: astro-ph/0011070 [astro-ph]. doi:10.1063/1.1363540 (2000).
59. The factor of 20 was also seen in the calculation of the Hubble constant when using values for the distances. In the FRW calculations, it is seen as two times the angle value and ten times the function value. The authors have no first principle explanation for the factor and therefore treat it as a calibration.
60. The quantity $a(t)$ that multiplies the spatial distance $dl = dr^2 + r^2(dq^2 + \sin^2q df^2)$ is called the scale factor of the universe. It describes how the spatial part of the universe expands or contracts. In an expanding universe $a(t)$ increases with time. This implies that the distance dl between any two nearby points increases by the factor $a(t)$ as the universe evolves
www.physics.fsu.edu/users/ProsperH/AST3033/Cosmology.htm
61. [https://en.wikipedia.org/wiki/Inflation_\(cosmology\)](https://en.wikipedia.org/wiki/Inflation_(cosmology))
62. .Hubble, Edwin) Proceedings of the National Academy of Sciences of the United States of America, **15**, 168–173 (1929)
63. casa.colorado.edu/~ajsh/phys5770_08/frw.pdf
64. A.G. Riess *et al.*, Astron. J. **560**, 49 (2001)
65. A. G. Riess and Michael S. Turner, Sci. Amer., **Feb.**, 62 (2004)
66. A, G. Riess and M. S. Turner, Sci. Amer., **Feb.**, 62 (2004)
67. A. G. Riess *et al.*, Astron. J. **116**, 1022 (1998)
68. A. G. Riess *et al.*, Astron. J. **560**, 49 (2001)
69. Adam G. Riess *et al.*, Astron. J. **116**, 1021 (1998)
70. Adam G. Riess *et al.*, Astron. J. **116**, 1021 (1998)

71. Adam G. Riess *et al.*, *Astron. J.* **116**, 1021 (1998)
72. A. G. Riess *et al.*, *Astron. J.* **116**, 1009 (1998)
73. A. G. Riess *et al.*, *Astron. J.* **116**, 1024 (1998)
74. A. G. Riess and Michael S. Turner, *Sci. Amer.*, **Feb.**, 66 (2004)
75. Science.nasa.gov > Astrophysics > Focus Areas
76. A. G. Riess *et al.*, *Astron. J.* **116**, 1020 (1998)
77. S. Perlmutter *et al.*, *Astron. J.* **517**, 571 (1999)
78. S. Perlmutter *et al.*, *Astron. J.* **517**, 570 (1999)
79. A. G. Riess *et al.*, *Astron. J.* **560**, 51 (2001), **560**, 63 (2001)
80. A. G. Riess *et al.*, *Astron. J.* **687**, 673 (2004)
81. S. Perlmutter *et al.*, *Astron. J.* **517**, 568 (1999)
82. casa.colorado.edu/~ajsh/phys5770_08/frw.pdf
83. S. Perlmutter *et al.*, *Astron. J.* **517**, 568 (1999); A. G. Riess *et al.*, *Astron. J.* **560**, 49 (2001)
84. A. G. Riess *et al.*, *Astron. J.* **116**, 1020 (1998)
85. S. Perlmutter *et al.*, *Astron. J.* **517**, 568 (1999)
86. A. G. Riess and M. S. Turner, *Sci. Amer.*, **Feb.**, 65 (2004)
87. Science.nasa.gov > Astrophysics > Focus Areas
87. A. G. Riess and Michael S. Turner, *Sci. Amer.*, **Feb.**, 66 (2004)
88. S. Perlmutter *et al.*, *Astron. J.* **517**, 570 (1999), **517**, 571 (1999)
89. A. G. Riess *et al.*, *Astron. J.* **677**, (2004)
90. A. G. Riess *et al.*, *Astron. J.* **665**, 673 (2004)

91. Anderson, J D.; Laing, P. A.; Lau, E. L.; Liu, A. S.; Nieto, M. M.; Turyshev, S. G. Phys. Rev. D **65** (2002) arXiv:gr-qc/0104064. Bibcode:2002PhRvD..65h2004A. doi:10.1103/PhysRevD .p.1.(082004)
92. Anderson, J D.; Laing, P. A.; Lau, E. L.; Liu, A. S.; Nieto, M. M.; Turyshev, S. G. Phys. Rev. D **65** (2002) arXiv:gr-qc/0104064. Bibcode:2002PhRvD..65h2004A. doi:10.1103/PhysRevD.p.19.(082004)
93. Anderson, J D.; Laing, P. A.; Lau, E. L.; Liu, A. S.; Nieto, M. M.; Turyshev, S. G. Phys. Rev. D **65** (2002) arXiv:gr-qc/0104064. Bibcode:2002PhRvD..65h2004A. doi:10.1103/PhysRevD.p.43.(082004)
94. Anderson, J D.; Laing, P. A.; Lau, E. L.; Liu, A. S.; Nieto, M. M.; Turyshev, S. G. Phys. Rev. D **65** (2002) arXiv:gr-qc/0104064. Bibcode:2002PhRvD..65h2004A. doi:10.1103/PhysRevD.p.43.(082004)
95. Abstract of the paper. We investigate the possibility that the anomalous acceleration of the Pioneer 10 and 11 spacecraft is due to the recoil force associated with an anisotropic emission of thermal radiation off the vehicles. To this end, relying on the project and spacecraft design documentation, we constructed a comprehensive finite-element thermal model of the two spacecraft. Then, we numerically solve thermal conduction and radiation equations using the actual flight telemetry as boundary conditions. We use the results of this model to evaluate the effect of the thermal recoil force on the Pioneer 10 spacecraft at various heliocentric distances. We found that the magnitude, temporal behavior, and direction of the resulting thermal acceleration are all similar to the properties of the observed anomaly. As a novel element of our investigation, we develop a parameterized model for the thermal recoil force and estimate the coefficients of this model independently from navigational Doppler data. We find no statistically significant difference between the two estimates and conclude that once the thermal recoil force is properly accounted for, no anomalous acceleration remains S.G.Turyshev, V.T, Toth, G. Kinsella, S. Lee, S.M.Lok and J. Ellis. Phys. Rev. Lett. **108**, 241101 (2012) arXiv:1204.250v1 p.1(4-11-21012)
96. M.M. Nieto and J.D.Anderson , arXiv:gr-qc/0507052v2, p.4.(10/4/2005)
97. M.M. Nieto and J.D.Anderson , arXiv:gr-qc/0507052v2, p.13.(10/4/2005)
98. M.M. Nieto and J.D.Anderson , arXiv:gr-qc/0507052v2, p.3.(10/4/2005)
99. M.M. Nieto and J.D.Anderson , arXiv:gr-qc/0507052v2, p.13.(10/4/2005)
100. M.M. Nieto and J.D.Anderson , arXiv:gr-qc/0507052v2, p.17.(10/4/2005)
101. M.M. Nieto and J.D.Anderson , arXiv:gr-qc/0507052v2, p.14.(10/4/2005)
102. M.M. Nieto and J.D.Anderson , arXiv:gr-qc/0507052v2, p.3.(10/4/2005)

103. The figure was redrawn for clarity.

M.M. Nieto and J.D.Anderson , arXiv:gr-qc/0507052v2, p.14.(10/4/2005)

104. Anderson, J D.; Laing, P. A.; Lau, E. L.; Liu, A. S.; Nieto, M. M.; Turyshev, S. G. Phys. Rev. D **65** (2002) arXiv:gr-qc/0104064. Bibcode:2002PhRvD..65h2004A. doi:10.1103/PhysRevD.p.19.(082004)

105. 91. Anderson, J D.; Laing, P. A.; Lau, E. L.; Liu, A. S.; Nieto, M. M.; Turyshev, S. G. Phys. Rev. D **65** (2002) arXiv:gr-qc/0104064. Bibcode:2002PhRvD..65h2004A. doi:10.1103/PhysRevD.p.19.(082004)

106. en.wikipedia.org/wiki/Doppler effect

107. The v_{∞} velocity (11.322km/s) for Pioneer 10 was taken at 5.02 AU after the Jupiter flyby. The v_{∞} velocity (10.45km/s) for Pioneer 11 was taken at 9.347AU after the Saturn flyby. This data is taken from Table 1 in the article.

M.M. Nieto and J.D.Anderson, arXiv: gr-qc/0507052v2, p.14. (10/4/2005)

108. Anderson, J D.; Laing, P. A.; Lau, E. L.; Liu, A. S.; Nieto, M. M.; Turyshev, S. G. Phys. Rev. D **65** (2002) arXiv:gr-qc/0104064. Bibcode:2002PhRvD..65h2004A. doi:10.1103/PhysRevD.p.42.(082004)

109 Anderson, J D.; Laing, P. A.; Lau, E. L.; Liu, A. S.; Nieto, M. M.; Turyshev, S. G. Phys. Rev. D **65** (2002) arXiv:gr-qc/0104064. Bibcode:2002PhRvD..65h2004A. doi:10.1103/PhysRevD.p.43.(082004)